NATIONAL ADVISORY COMMITTEE FOR AERONAUTICS

TECHNICAL NOTE 4220

A FLIGHT EVALUATION AND ANALYSIS OF THE EFFECT OF ICING CONDITIONS ON THE ZPG-2 AIRSHIP

By William Lewis and Porter J. Perkins, Jr.

Lewis Flight Propulsion Laboratory
Cleveland, Ohio

Washington
April 1958

NATIONAL ADVISORY COMMITTEE FOR AERONAUTICS

TECHNICAL NOTE 4220

A FLIGHT EVALUATION AND ANALYSIS OF THE EFFECT OF ICING CONDITIONS ON THE ZPG-2 AIRSHIP

By William Lewis and Porter J. Perkins, Jr.

SUMMARY

A series of test flights was conducted by the U. S. Navy over a 3-year period to evaluate the effects of icing on the operation of the ZPG-2 airship. In supercooled clouds, ice formed only on the forward edges of small protuberances and wires and presented no serious hazard to operation. Ice accretions of the glaze type which occurred in conditions described as freezing drizzle adversely affected various components to a somewhat greater extent. The results indicated a need for protection of certain components such as antennas, propellers, and certain parts of the control system.

The tests showed that icing of the large surface of the envelope occurred only in freezing rain or drizzle. Because of the infrequent occurrence of these conditions, the potential maximum severity could not be estimated from the test results. The increases in heaviness caused by icing in freezing rain and drizzle were substantial, but well within the operational capabilities of the airship.

In order to estimate the potential operational significance of icing in freezing rain, theoretical calculations were used to estimate: (1) the rate of icing as a function of temperature and rainfall intensity, (2) the climatological probability of occurrence of various combinations of these variables, and (3) the significance of the warming influence of the ocean in alleviating freezing-rain conditions. The results of these calculations suggest that, although very heavy icing rates are possible in combinations of low temperature and high rainfall rate, the occurrence of such conditions is very infrequent in coastal areas and virtually impossible 200 or 300 miles offshore.

INTRODUCTION

The nonrigid airship ("blimp") has been adapted to carry aircraft detection equipment for use in the air defense system. The aircraft-early-warning mission requires that picket aircraft endure all types of

weather conditions while maintaining a continuous watch from a particular area. In support of this mission a project was established by the Office of Naval Research to evaluate the all-weather capabilities of the ZPG-2 airship (975,000 cu ft envelope)(fig. 1). The flight testing was assigned to the Naval Air Development unit at the United States Naval Air Station in South Weymouth, Massachusetts. The NACA Lewis laboratory was requested by the Office of Naval Research to assist the Navy by supplying instrumentation and technical assistance in analyzing and studying the icing problem as applied to airships.

Weather conditions considered hazardous to airborne operations are those conducive to ice and snow accumulations on various parts of the airship and those affecting the operational capability of the airship, such as winds and turbulence. The flight tests and study reported herein were conducted only for the purpose of investigating the airworthiness of the airship in various types of icing conditions.

Previous airship operations in patrol and convoy duty were not seriously confronted with the icing problem because these missions were flown at altitudes (50 to 500 ft) below the levels of most icing clouds. Icing and snow problems of most concern for early airships were mostly confined to difficulties encountered during outside mooring on the mast. The added weight of ice and snow accumulations on the top of the envelope would buckle the landing gears and in cross winds would cause the airship to roll to one side and damage outriggers and fins. The in-flight ice and snow problem was investigated to a limited extent in 1945 when the NACA assisted the Navy in a preliminary study of ice-protection requirements for the K-type airship (435,000 cu ft envelope). The results are reported in reference 1 for a $2\frac{1}{2}$-hour flight in conditions described as being a mixture of wet snow and freezing rain and which produced no adverse effects on the operation of the airship. The icing and snow problem has become relevant to the present ZPG-2 airship with its increased altitude range in the aircraft-early-warning mission which places operations more frequently at levels of icing clouds.

The flight tests reported herein were conducted over a period of three icing seasons along the coast of the northeastern United States. A completely unprotected ZPG-2 airship was flown in icing conditions during the first two winters. A second similar airship incorporating limited icing protection based on experience gained from the earlier flights was used during the final season. Test objectives were to determine the components of the airship which collect ice and the resulting effects on operation and performance. Flights were also planned to evaluate the ice and snow problem over water. The first part of this report describes several flights in a variety of ice and snow conditions and the resulting effects on various components as reported by Naval Air Development unit personnel.

A preliminary study of the airship icing problem indicated that accumulations of ice or snow on the large surface areas along the top of the envelope and fins could produce the serious problem of weight greater than the lifting capacity of the airship. This problem would exist only in the more unusual conditions of freezing drizzle or rain where the drop sizes are of sufficient size to strike the envelope surface. Droplets in the smaller size range of supercooled clouds (<100 microns) would not impinge on the envelope in sufficient amounts to be of concern. The low airspeed and gradual curvature of the large airship envelope allow the small light-weight droplets to be easily deflected by the airstream around the envelope. Atmospheric conditions encountered during the flight tests did not provide sufficient information to evaluate this primary problem of ice loads from freezing rain adequately. It was considered advisable, therefore, to calculate rates of ice formation on the airship envelope based on theoretically derived droplet trajectories and heat-transfer relations combined with rainfall rates and temperatures typical of freezing-rain conditions. The operational significance of this problem during offshore missions was also considered desirable. The second part of this report presents the results of these calculations, including an analysis of the probability of freezing rain for offshore areas.

DESCRIPTION OF TEST AIRSHIP AND INSTRUMENTATION

The ZPG-2 airship used in the tests (fig. 1) has a fabric envelope filled with approximately 975,000 cubic feet of helium. The over-all length is 342 feet and the maximum diameter is 75 feet. Two 18-foot propellers are mounted on outriggers projecting from each side of the car. Power is transmitted through shafting from the engines mounted inside the car. The stabilizers and control surfaces (ruddevators) are mounted at 45° angles and are supported by brace wires attached to the envelope surface. Exposed control cables run from the car to the ruddevators. The airship is normally operated in a heavy condition (i.e., heavier than the air displaced by the envelope) and thus requires some dynamic lift for flight.

The test instrumentation consisted of equipment to measure and observe ice accretions on various airship components and to evaluate the effects of the ice on the operation of the airship. Rate-of-accretion meters indicated the magnitude of ice formations on the forward edges of small exposed components. These meters recorded the rate at which ice formed on the leading edge of a thin rotating disk and were used in flight to detect the presence of icing and the duration of the icing conditions (see ref. 2 for a description of these meters). Ice deposited per unit area on the top surfaces of the envelope in freezing rain or drizzle was measured at three locations (nose, center, and tail sections) by use of a device developed specifically for this purpose by the Clevite

Brush Company. This instrument utilized the change in resonant frequency caused by ice accumulating on a vibrating sensing element mounted flush with the surface. The frequency change of piezo-electric driving stacks contained in the sensing elements was measured electronically. Only preliminary development of this instrument was accomplished during the program. The rotating-multicylinder technique was employed during part of the program to measure droplet sizes and liquid-water content of the icing clouds. Ice formations on areas not visible from the car were observed with movie cameras mounted at several points throughout the airship and with a television camera installed on the top to view the aft section.

Flight conditions were either recorded on film or observed by the crew. Outside air temperature, altitude, and airspeed were continuously recorded. The flying qualities of the airship under test conditions were judged mainly by the pilot. For most flights the handling characteristics and increased load caused by the ice accretions were estimated by relating angle of attack, airspeed, and power settings to those required for normal ice-free operation.

DISCUSSION OF ICING FLIGHTS

Icing conditions of sufficient intensity and duration to provide pertinent results were encountered on nine airship flights along the coast of the northeastern United States during three icing seasons. Table I summarizes the data from these flights using the records from the disk-type icing-rate meters to evaluate the icing conditions. Rime ice was encountered on six flights and freezing rain or drizzle was present during three icing encounters. The rime ice, resulting from small supercooled cloud droplets, formed only on exposed objects and protuberances and not on the large envelope surface. The freezing-drizzle conditions, where the droplet sizes were much larger, produced a film of ice on the top envelope surfaces as well as glaze-ice formations on exposed components. Compared with the rime-ice encounters, the freezing drizzle produced somewhat more deleterious effects on the operation of the airship. The many factors, including droplet size, which influence the ice collection characteristics of various sized objects are discussed in a later section.

Flights in Freezing Rain and Drizzle

The largest total amount of ice measured during the program was accumulated on flight number 3. Glaze-ice formations were produced from a condition described as freezing drizzle. Although droplet sizes were not measured, the flight reports and ground observations indicated the airship was flown in clouds in an area of light precipitation.

The increasing ice accumulation with time as measured by the icing-rate meters is shown in figure 2 for a chronology of events reported during the flight. Icing was encountered during climb shortly after takeoff from South Weymouth. The greatest icing rate appeared to be at the 3000-foot level where the temperature was -1.5° C and the visibility very limited. After 25 minutes of continuously increasing ice accumulation at this altitude, a slight vibration of the car was noted. About 5 minutes later this vibration became excessive and caused the instrument panel to shimmy up to the limits of its shock mounts. The frequency of the car vibration was estimated as about 5 cycles per second. During this period ice thrown from the propellers was heard striking the sides of the car which suggested that propeller unbalance may have been present. These pieces of ice also caused a rip in the fabric fairing between the car and envelope. The vibration diminished during the following 10 to 15 minutes, then increased again and became very pronounced about 5 minutes later. A descent was made shortly thereafter out of the icing level into above freezing temperatures. The airship had been exposed to continuous icing for about 70 minutes. The clear ice formed under these conditions is illustrated in figure 3, which shows ice formations on the yawmeter mounted below the pilot's window.

During the descent sheets of ice began sliding off the envelope from the bow area and falling back into the propellers and windshield. Ice was also noted falling from other areas along the sides of the envelope during the approach to the runway. The surface-ice accretion meters were inoperative during this flight, and therefore the envelope ice load was not measured. A total ice load of about 4000 pounds was estimated by considering airspeed, deck angle, and power settings. This included the accumulated ice on fin brace wires and protuberances as well as on the envelope surface.

Near the end of the icing period the fin brace wires were observed oscillating at an estimated 6-inch amplitude. Ice accretions up to $1\frac{1}{2}$ inches in diameter had formed on the 3/16-inch-diameter wires. Some flapping motion of the fins was also detected. The control cables had also collected some ice, but their operation was not impaired. An inspection upon landing revealed some 30 punctures in the fabric surfaces of the two lower fins. These 1- to 6-inch punctures were attributed to pieces of ice thrown from the oscillating brace wires or to chunks of ice falling from the leading edge of the upper fins or both.

Other operational problems resulting from the icing included the freezing shut of an air damper controlling air to the center ballonet and ice on the windshield which completely obscured forward visibility. Operation of the damper by either electrical or manual controls was not possible. The windshield defogging system was ineffective in preventing or removing the ice coating.

The car vibration was attributed to propeller unbalance caused by uneven throwoff of ice from the individual blades. A propeller unbalance could produce a greater airframe vibration on the ZPG-2 airship than on a conventional aircraft because of the propeller mounting configuration. Since the propellers are rigidly mounted to the outrigger frames without shock mounts, vibrations from unbalance can be easily transmitted throughout the airframe. Also, the cantilever design of the low-mass outrigger structures allows for marked increases in the amplitude of forced vibrations under conditions of resonant frequencies.

Another flight in freezing-rain conditions (flight number 4, table I) produced only small ice accretions at temperatures slightly below freezing. Intermittent periods of icing existed at the freezing level for about 30 minutes. Wires and protuberances collected a slight amount of ice. After the airship left the precipitation area, water ran off the envelope, which indicated some ice had formed on the top surfaces. The ice load was not estimated.

A vertical sounding was made during this flight to determine the depth of the freezing-rain level. Rain at above freezing temperatures was falling at the ground at the time of takeoff. Low ceilings (150 ft) and visibilities (1/2 mile) were prevalent in the area of the flight. During climb the temperature decreased to freezing at 1700 feet, but at 3000 feet the temperature was again above freezing. Hence, the layer of freezing rain was less than 1500 feet deep. The inversion continued to be observed up to the altitude limit of the airship of 5000 feet where light rain was falling.

The only other icing encounter in which freezing drizzle was present occurred during flight number 5 (table I). Since the flight was in clouds, supercooled cloud droplets may have contributed to the ice formations. Effects on the airship were similar to those described for flight number 3, although total ice accumulations were not as great. In 6 hours of flight icing occurred during three separate periods, each approximately 40 minutes in duration. The encounters were separated by a sufficient time lapse (1 to 2 hr) at above freezing temperatures to allow most of the ice formed during the previous encounter to melt. The ice buildup recorded by the icing-rate meters for each icing period is shown in figure 4.

The first period of icing (flight 5, encounter (a), fig. 4) occurred at 2400 feet (at -1° C) during climb over South Weymouth in conditions described as freezing drizzle. As the maximum buildup of ice was reached (1/4 in. recorded by an icing-rate meter), slight car vibration was felt which was attributed to propeller icing. Ice also formed on the antennas (causing vibrations), on the windshield, on the radome, and on other components. After about 3/4 hour the shallow freezing layer in the inversion decreased in thickness to the points where melting began.

During the next $1\frac{1}{2}$ hours the airship proceeded to the Cape Cod area where icing again was encountered. All ice accretions from the previous encounter had melted. Vibration again was felt when about 1/4 inch of ice had accumulated. Excessive antenna whipping was also present. When maximum accretion was reached (about 1/2 in. in 30 min), there was excessive vibration of the car for about 5 minutes. This was accompanied by propeller ice throwoff. A climb at this point to 3200 feet produced melting at 1° C, which indicated that an inversion was also present in this icing area. As the melting continued, ice in thin sheets fell from the sides of the envelope and struck the propeller, the outriggers, and the windshield.

The third icing condition was entered upon return to the South Weymouth area at 3000 feet. This condition was similar to the first encounter of the flight in that only 1/4 inch of ice accumulated over a 40-minute period. Antenna whipping again appeared excessive. Airspeed was reduced to help prevent the wires from snapping. Inspection of the airship after landing disclosed ice accretions 1/2 to 3/4 inch thick on the fin brace wires and control cables, but no ice had remained on the envelope surface.

During a takeoff on the day following this flight, a control problem arose which was considered related to the icing encountered on the previous day. In an attempt to climb the airship veered sharply to the right. Flight was maintained, however, and a landing was effected with the controls still fouled. Inspection showed that movement of the lower left ruddevator was prevented by the control cable, which had jumped a pulley and lodged between the pulley and its guard. The failure was assumed to have developed during the rollout phase of the landing from the previous flight. A buildup of ice on the affected cable and pulley would cause no trouble for normal flight, because the control movements are usually small. However, the large cable travel required on landing could cause the enlarged cable to ride up and out of the iced-over pulley groove. A similar control-system difficulty was encountered during flight number 6 also. When the automatic pilot was disengaged prior to letdown, movement of the controls was dangerously restricted. They could be moved manually only in small increments. Complete control was regained after descent into above freezing temperatures.

Flights in Rime Ice

The rime icing conditions were found in typical supercooled clouds with temperatures ranging from -2° to -10° C and liquid-water contents from 0.1 to 0.5 gram per cubic meter. The ice formations were different from those produced in freezing drizzle in that the rime accretions were confined to the forward edges of small objects only and, unlike glaze-ice formations, had less tendency to spread. A comparison of the two types of ice formation is shown in the flight photographs of figure 3.

The initial flight in rime icing conditions (flight number 1, table I) revealed the antenna whipping problem. Of particular concern at the time was the possibility of an antenna breaking. Had the starboard antenna broken near the forward mount, the wire could have tangled with the ripcord and whipped back into the propeller, pulling the ripcord with it. (The ripcord is an emergency device which when pulled tears an opening in the top of the envelope to allow rapid escape of the helium. The purpose is to destroy aerostatic lift rapidly in emergency situations developing at or near the ground.)

The second airship, which was flown during the final season of the project, encountered only rime icing conditions in operations intended to evaluate the ability of the airship to conduct various missions. Test objectives were (1) to evaluate extended flights over water (24 hr or more) simulating patrol missions in conditions favorable for icing, (2) to demonstrate "barrier" station operations for an extended period (10 days), and (3) to conduct a distance-endurance flight following a circuitous route around the northern Atlantic Ocean (8200 miles in 11 days). In the icing conditions encountered during these missions no adverse effects on airship operations were noted, and no potentially hazardous situations developed.

This airship was provided with limited icing protection based on the flight experiences with the original test airship. Modifications considered most desirable and installed on the airship included:

(1) A shielded control cable system (at ruddevator horn pulleys only)

(2) Flush-mounted antennas

(3) Electrically heated propellers (external rubber boots)

(4) Electrically heated center-ballonet air-inlet dampers

(5) Increased hot air to the windshield

(6) Added strength (protective coating) to the fabric covering top surfaces of lower fins

(7) A protective blanket inside the envelope in the plane of the propellers

Flight number 8 (table I), which was conducted in support of the 10-day barrier operation, encountered prolonged periods of rime icing while holding in the area. The airship was in clouds and snow during most of the 40-hour flight. Synoptic data indicated a situation of mixed clouds (supercooled water changing to ice crystals and snow) formed by very

cold air over a warm sea surface. Icing occurred in four separate periods with an estimated cumulative time in icing of about 5 hours. Ice accretions (about $1\frac{1}{4}$ in.) were the largest recorded for rime icing encounters. The pilot noted that the ice on small protuberances would build up to a certain thickness and break off. Thus, it would seem that this condition approached the maximum effect of prolonged periods of rime icing. The total ice load was estimated not to have exceeded 2000 pounds. Some snow in the tail section contributed to the increased heaviness.

In general, the over-all operation of the airship was not seriously impaired by the rime icing conditions that were encountered. The limited icing protection installed on the second airship appeared adequate for those components which were adversely affected by the rime accretions.

Flights in Snow

Several flights were conducted in moderate to heavy snow with little or no in-flight effects on the airship. Snow loads accumulated while an airship is on the mast have long been recognized as a serious problem. In flight, however, most of the snow catch blows off at the higher airspeeds, except possibly very wet snow. The results of a 2-hour flight in light to moderate snow at -2° to -6° C are shown in figure 5(a). A small catch estimated to be about 1000 pounds can be seen distributed along the top of the envelope and in the catenary seam along the side. On other flights snow was observed only on the top, between and aft of the fin area, as shown in figure 5(b).

During the test flights snow loads created operational problems on two occasions. While the airship was on the mast prior to takeoff for flight number 9, a heavy snow load collected on the top. Although some snow blew off during takeoff, the airship remained very tail-heavy and required all ballonet air forward plus the elevator down to effect a 13° angle of attack at 2000 feet. The airship was operating at maximum gross weight and low power settings to minimize fuel consumption because of the endurance requirements of the mission. About 20 minutes of icing was encountered soon after takeoff, which produced a small accumulation (0.1 in.). The combined effect of all these conditions created a stall situation which required descent to a lower altitude. This provided increased ballonet air capacity, which was used to reduce the high angle of attack. With less down elevator also reducing the drag, level flight could be maintained without an increase in power.

Heavy snow produced another problem during a special maneuver conducted while on a barrier station. An attempt to pick up sea-water ballast was abandoned when altitude could not be maintained at the very low

ground speeds required for this operation. The crew concluded that with light surface winds (7 to 9 knots) the low airspeed allowed snow to accumulate, whereas at higher airspeeds the snow would blow off. Another consideration was that warmer temperatures near the sea surface produced wet snow which adhered to the top surfaces better.

THEORETICAL ANALYSIS OF AIRSHIP ICING IN FREEZING RAIN

The flight-test results confirmed the prediction from theory that heavy ice loads on the envelope occur only in freezing rain or drizzle. Because of the low frequency of occurrence of freezing rain, insufficient experience was obtained to provide a reliable basis for estimating maximum icing rates. It appeared desirable, therefore, to resort to calculations to determine the relation between icing rate and meteorological conditions, in order that climatological data might be used to evaluate the operational significance of icing in freezing rain.

Calculation of Rate of Icing in Freezing Rain

The rate of ice formation per unit area at a given location on the airship envelope depends on the rate of water impingement, the airspeed, and the wet-bulb temperature of the air. The temperature dependence results from the fact that, as ice is formed, the latent heat must be removed by convective transfer to the environment. For any combination of airspeed, temperature, and location on the airship there exists a critical freezing rate at which the release of latent heat is just sufficient to raise the surface temperature to 32° F. If the water impingement rate is less than the critical freezing rate, all the water freezes, and the icing rate equals the impingement rate. If the impingement rate is greater, most of the excess water runs off in the liquid state.

In order to determine the total rate of ice formation on the envelope for a given combination of airspeed, rainfall rate, and wet-bulb temperature, it is necessary to calculate the distribution of water impingement rate and critical freezing rate over the envelope surface. The distribution of impingement has been determined as a function of rainfall rate and airspeed by assuming that the impingement is the sum of two terms: (1) the gravitational impingement that would occur if the airship were at rest in still air and (2) the dynamic impingement that would result from forward speed alone, neglecting gravity. The distribution of the critical freezing rate was calculated from heat- and mass-transfer equations based on references 3 and 4. Both sets of calculations are described in appendix B (symbols are defined in appendix A). A comparison of critical freezing rate and impingement rate, expressed in pounds per hour per foot along the axis, for a particular set of conditions is shown in figure 6(a). At locations where the

critical freezing rate is greater than the impingement rate, all the impinging water freezes, and the icing rate equals the impingement rate. Where the impingement rate exceeds the critical freezing rate, the icing rate is greater than the critical freezing rate by the amount of ice formation required to release sufficient latent heat to raise the temperature of the excess water to 32° F.

For example, in figure 6(a) at a location of 60 feet from the nose the impingement rate (33 (lb/hr)/ft) is less than the critical freezing rate (44 (lb/hr)/ft), and the icing rate is equal to the impingement rate (33 (lb/hr)/ft). At a location 20 feet from the nose, on the other hand, the impingement rate (117 (lb/hr)/ft) is greater than the critical freezing rate (67 (lb/hr)/ft). The excess water (50 (lb/hr)/ft) undergoes a temperature rise from 27° to 32° F, which absorbs heat at a rate of 50x5 or 250 (Btu/hr)/ft, and thus freezes additional ice in the amount of 250/144 or 1.7 (lb/hr)/ft. The local icing rate is therefore 67 + 1.7 or 68.7 (lb/hr)/ft.

The total icing rate for the entire envelope is found by integrating the local icing rate over the total length. In the coordinates of figure 6(a), this integration is accomplished by determining the area under both the impingement-rate and critical-freezing-rate curves, using whichever curve is lower at any location. To this area is added $(32 - t_{kw})/144$ times the area lying <u>below</u> the impingement curve and <u>above</u> the critical-freezing-rate curve.

Figure 6(b) shows how the relation between impingement and critical freezing rate changes as the rainfall rate increases at constant temperature and airspeed. At rainfall rates up to 0.04 inch per hour, for the conditions shown in figure 6(b)(28° F, 30 knots), the area of excess impingement and runoff comprises only a small portion of the envelope at the nose. Thus, the icing rate increases almost linearly with the rainfall rate. At a rainfall rate of about 0.047 inch per hour runoff sets in along the rear half of the envelope about 250 feet from the nose, and at a rainfall of 0.05 inch per hour most of the rear half is running wet. Beyond this point the icing rate increases more slowly with increasing rainfall. Finally, beyond 0.075 inch per hour the entire envelope is subject to runoff, and further increases in rainfall cause only a small increase in icing. Curves such as those shown in figure 6 provide a means of estimating the total icing rate as a function of rainfall rate for a given airspeed and temperature, as shown in figure 7.

Effect of Climatic Factors on Probable Frequency and Severity of Icing in Freezing Rain

The calculated rates of icing presented in figure 7 show that very heavy ice loads can be collected in periods of an hour or less in certain combinations of temperature and rain intensity. The operational significance of these results depends on the frequency of freezing rain and the relative frequency of various combinations of temperature and rainfall rate in freezing rain. These are climatic factors, varying with geographical location and season.

The occurrence of freezing rain requires the presence of a low-altitude layer of air at temperatures below freezing surmounted by a layer of warmer air in which the temperature is above the melting point. When a shallow layer of cold air flows over relatively warm water, the surface-air temperature rapidly approaches that of the water. Heat-transfer calculations described in appendix C show that the existence of conditions required for freezing rain at low altitudes over the sea is virtually impossible in air that has had a trajectory of approximately 300 miles or more over water at a temperature of 45° F or higher. In the light of this result, an examination of the January sea-surface temperature distribution (fig. 8) shows that the only potential icing areas that need be considered with reference to the aircraft-early-warning mission are the coastal areas of the northeastern United States and the adjacent ocean areas.

Frequency of occurrence of freezing rain in northeastern United States. - The estimated average frequency of occurrence of freezing rain in winter in the northeastern United States is shown in figure 9. The data shown are 3-month (December through February) average percentages based on two daily observations at 12 stations with an average record length of 9 years. These values were obtained from an unpublished listing of freezing-level and surface-temperature data for freezing precipitation furnished by the National Weather Records Center. The general pattern of freezing-rain frequency shows a gradual increase from south to north and a rapid decrease along the coast. This strong coastal effect is the result of the warming influence of the ocean in cases in which an onshore component exists in the cold-air flow.

Probable maximum airship icing rates in freezing rain over land area in northeastern United States. - Since the icing rate is a known function of airspeed, rainfall rate, and free-air temperature, the frequency distribution of icing rates for a given airspeed can be calculated from the frequency distributions of temperature and rainfall rate. The frequency distribution of surface-air temperatures reported during freezing rain is shown in figure 10 (data from the same source as fig. 9). Surface-air temperatures are probably representative of flight temperatures for

aircraft-early-warning airship operation over land at low altitudes during return to or departure from the base. An estimated frequency distribution of rainfall rate applicable to freezing rain is shown in figure 11. The method of selecting data and the theory underlying their use to represent freezing rain are given in appendix D.

Combining the temperature distribution of figure 10, the rainfall distribution of figure 11, and the relation between icing rate and temperature and rainfall rate shown in figure 7 yields the frequency distributions of icing rate shown in figure 12 for airspeeds of 30 and 50 knots. Thus, if an airship is flying at 30 knots in freezing rain, the chances are 1 in 10 that the icing rate exceeds 6300 pounds per hour and 1 in 100 that it exceeds 14,000 pounds per hour. The temperature and rainfall distributions would not be expected to vary widely in the limited geographical area of the northeastern United States because the occurrence of freezing rain fixes the air-mass temperatures within rather narrow limits. Thus, figure 12, which gives the probability of various icing rates when freezing rain is known to be occurring, may be regarded as applicable generally to land areas near the east coast of the United States in winter. The geographical effects within this area are included in the frequency of occurrence of freezing rain (fig. 9).

Estimated conditions off northeastern coast of United States. - As implied in figure 9, the probability of encountering freezing rain is much less over the ocean off the coast of the northeastern United States than it is over adjacent land areas. Since direct observations of freezing-rain frequencies at sea are not available, it is desirable to estimate the effect of flow over the relatively warm sea surface in modifying the air-mass temperature structure in freezing-rain situations.

An analysis of heat transfer occurring when a layer of cold air topped by an inversion flows over a warm water surface is presented in appendix C. The distance of travel over the ocean (surface temperature, 6° C) required to raise the surface-air temperature to 2° C was calculated as a function of the initial surface-air temperature and the height of the first freezing level. A surface-air temperature of 2° C was chosen as representing a condition under which an airship could safely descend to below the freezing level (about 700 ft) and shed accumulated ice. The relative frequency of various combinations of surface-air temperature and height of the first freezing level measured during freezing rain were combined with the calculated values of distance to 2° C to obtain the frequency distribution shown in figure 13. This curve shows the percentage of cases of freezing rain (observed on land) that would be warmed sufficiently to have a surface-air temperature of 2° C or higher as a function of distance transported over water at 6° C. Thus, one-half of the freezing-rain cases at the coast would be effectively eliminated at 64 nautical miles offshore, 90 percent at 145 miles, and 99 percent at 260 miles.

In interpreting these results, it should be noted that synoptic experience has shown that most cases of freezing rain on land are not transported directly out to sea. Thus, figure 13 overestimates the hazard, since it is based on the assumption that all freezing-rain situations move out to sea.

CONCLUDING REMARKS

In test flights conducted by the Navy to evaluate the effects of ice accretions on the ZPG-2 airship a number of typical icing conditions were encountered. While the airship was exposed to these conditions, ice formed on various components but presented no serious hazard to the operation of the airship, although some potentially unsafe situations developed. The more common rime ice formed only on the forward edges of small protuberances and wires without causing appreciable concern. Ice accretions of the glaze type which occurred in what was described as freezing drizzle adversely affected various components to a somewhat greater extent. Protective designs for some of the affected components appeared desirable to assure safe operations.

A study of the ice accretion problem for airships indicated that in addition to component icing a problem could develop from an excessive ice load on the large surface area along the top of the envelope which would occur only in conditions of freezing rain. This potentially hazardous situation was not adequately investigated in the flight tests because of the infrequent occurrence of these conditions. However, the tests verified that ice can form on the top of the envelope when the drop sizes approach those characteristic of freezing rain. During these flights the ice formations did not produce a sufficient increase in airship heaviness to become an operational problem.

The calculations presented in this report show that very heavy ice loads can be collected under more extreme conditions of rain intensity and temperature than those encountered during the flight program. The operational significance of these hazardous conditions depends on the frequency of their occurrence. In a search for all types of inclement weather the flight test program demonstrated the low probability of these situations occurring over land areas along the northeastern coast of the United States. The probability is further evaluated in this report using several years of meteorological data from land areas.

The calculated icing probability curves and the calculated effect of warming over the sea are somewhat speculative. Actual numerical values are therefore uncertain, but the following qualitative conclusions of operational significance may be stated with considerable confidence:

(1) It is possible to encounter very heavy rates of icing under conditions of high rainfall rate and low temperature.

(2) Statistics on rainfall rate and temperature in freezing rain indicate that combinations giving rise to hazardous icing rates may be expected in from 1 to 5 percent of freezing-rain occurrences over land areas in the northeastern United States. Since freezing rain occurs in this area in only about three to five storms per year, the probability of severe icing is very small.

(3) Because of the warming effect of the sea surface, the probability of encountering hazardous icing in freezing rain decreases rapidly with distance offshore, becoming negligible at 200 to 300 miles.

(4) The effect of freezing rain in aircraft-early-warning operations is likely to be confined to arrivals and departures, when the airship is over land or a short distance offshore. Hazardous icing during these phases of operation can probably be avoided with the aid of weather forecasts, since the synoptic conditions required for freezing rain can be forecast satisfactorily for short periods.

Lewis Flight Propulsion Laboratory
National Advisory Committee for Aeronautics
Cleveland, Ohio, December 17, 1957

APPENDIX A

SYMBOLS

A_f	frontal area of airship, sq ft
A_h	horizontal projected area of airship, sq ft
c_p	specific heat of air at constant pressure, Btu/(lb mass)(°F), kcal/(kg)(°C) in appendix C
D_z	diameter of envelope at distance z from nose, ft
E	collection efficiency, dimensionless
F_{cr}	critical freezing rate per unit distance along axis, lb mass/(hr)(ft)
f_{cr}	critical freezing rate per unit area, lb mass/(hr)(sq ft)
H	heat-transfer coefficient, Btu/(hr)(sq ft)(°F), kcal/(hectare)(hr)(°C) in appendix C
H_c	convection heat-transfer coefficient, kcal/(hectare)(hr)(°C) (appendix C)
H_r	radiation heat-transfer coefficient, kcal/(hectare)(hr)(°C) (appendix C)
$h_{i,32}$	specific enthalpy of ice at 32° F, Btu/lb mass
$h_{l,kw}$	specific enthalpy of liquid water at kinetic wet-bulb temperature, Btu/lb mass
$h_{l,w}$	specific enthalpy of liquid water at wet-bulb temperature, Btu/lb mass
$h_{v,kw}$	specific enthalpy of water vapor at kinetic wet-bulb temperature, Btu/lb mass
$h_{v,32}$	specific enthalpy of water vapor at 32° F, Btu/lb mass
J	mechanical equivalent of heat, ft-lb/Btu
k	thermal conductivity of air, Btu/(hr)(ft)(°F)
M	total rain impingement rate, lb mass/hr

M_d	dynamic impingement, lb mass/hr
M_g	gravitational impingement, lb mass/hr
m_d	dynamic impingement per unit length, lb mass/(hr)(ft)
m_g	gravitational impingement per unit length, lb mass/(hr)(ft)
Nu	Nusselt number, dimensionless
P	atmospheric pressure, mb
Pr	Prandtl number, dimensionless
p_{kw}	saturated vapor pressure over liquid water at t_{kw}, mb
p_o	free-stream vapor pressure, mb
p_{32}	saturation vapor pressure at 32° F, mb
Q_v	heat of vaporization of water, kcal/kg (appendix C)
q_a	increase in enthalpy of cold-air layer, kcal/(hectare)(hr)
$q_{as,c}$	heat loss from airship surface by convection, Btu/(hr)(sq ft)
$q_{as,e}$	heat loss from airship surface by evaporation, Btu/(hr)(sq ft)
$q_{as,fr}$	heat liberated at airship surface by freezing, Btu/(hr)(sq ft)
$q_{ss,c}$	heat loss from sea surface by convection, kcal/(hectare)(hr)
$q_{ss,e}$	heat loss from sea surface by evaporation, kcal/(hectare)(hr)
$q_{ss,r}$	heat loss from sea surface by radiation, kcal/(hectare)(hr)
R	rainfall rate, in./hr
Re	Reynolds number based on surface distance s, dimensionless
r	temperature recovery factor, dimensionless
St_c	Stanton number for convection, dimensionless
St_r	Stanton number for radiation, dimensionless
s	distance along airship surface from nose, ft
T_{cond}	temperature at condensation level, $^\circ C$

T^*_{cond}	temperature at condensation level, ^oK
T_d	temperature on dry adiabatic line through T_c, ^oC
T_o	surface-air temperature, ^oC
$T_{o,cl}$	surface-air temperature at coast line, ^oC
$T_{o,y}$	surface-air temperature after trajectory of length y, ^oC
T_{ss}	sea-surface temperature, ^oC
T^*_{ss}	sea-surface temperature, ^oK
T_w	temperature in cloud above condensation level, ^oC
t_{ki}	kinetic iced-bulb temperature, ^oF
t_{kw}	kinetic wet-bulb temperature, ^oF
t_o	free-stream temperature, ^oF
U_s	local airspeed outside boundary layer, ft/sec
U_o	free-stream velocity, ft/sec
V	airspeed or wind speed, knots
v	raindrop falling speed, knots
w	liquid-water content in rain, lb mass/(sq ft)(nautical mile)
x_l	liquid-water mixing ratio, g water/g air
x_t	total water mixing ratio, g water/g air
x_v	water-vapor mixing ratio, g water/g air
$x_{v,sat}$	saturation water-vapor mixing ratio over sea water at T_s
y	distance over ocean, nautical miles
Z	height above sea surface, hectometers
Z_{cond}	height of condensation level, hectometers
Z_{fr}	height of freezing level in inversion, hectometers

Z_{ib}	height of inversion base, hectometers
Z_p	pressure altitude, ft
z	distance from nose, measured along axis, ft
z_m	axial distance to limit of dynamic impingement, ft
α	ratio of dynamic to gravitational impingement, dimensionless
θ	depression of kinetic wet-bulb temperature below freezing, ^{o}F
λ	wetted-area factor, dimensionless
μ	viscosity of air, lb mass/(ft)(sec)
ρ	density of air, lb mass/cu ft, kg/(hectometer)^3 in appendix C
ρ_o	density of air at sea level, kg/(hectometer)^3
$\bar{\rho}$	average air density from sea level to height of inversion base, kg/(hectometer)^3
σ	Stefan-Boltzmann constant, kcal/(hr)(hectare)(^{o}K)^4
τ	time, hr
Φ	thermodynamic heat-transfer function defined in eq. (B11), lb mass/(hr)$^{0.2}$(ft)$^{1.8}$(nautical mile)$^{0.8}$

APPENDIX B

CALCULATION OF AIRSHIP ICING RATE IN FREEZING RAIN

The calculations presented herein apply to the "theoretical envelope" only and do not include icing of the car, fins, brace cables, and so forth.

Impingement of Rain on Airship Envelope

In estimating the rate and distribution of rain impingement on an airship it is necessary to consider two processes, gravitational settling and dynamic interception. These two processes are not independent, because gravitational settling is modified by the local airflow about the airship, and the dynamic impingement is influenced by the effect of gravity on the raindrop trajectories. Because of the difficulties involved in an analytical treatment of combined gravitational and inertial impingement, and since trajectory calculations neglecting gravity were at hand, the two effects were evaluated independently, with the assumption that the total impingement is equal to two terms: (1) the gravitational impingement M_g that would occur if the airship were at rest in still air, and (2) the dynamic impingement M_d that would occur if the airship were moving through a field of raindrops suspended in air in the absence of gravity.

The gravitational impingement is a function of the rainfall rate and the projected area. Since 1 inch of rain equals 5.2 pounds per square foot, the total gravitational impingement is given by

$$M_g = 5.2\ RA_h \tag{B1}$$

The gravitational impingement per foot of length measured along the axis of the envelope is

$$m_g = 5.2\ RD_z \tag{B2}$$

The distribution of gravitational impingement along the length of the airship is represented by m_g/R (lb/(ft)(in. rain)), as shown in figure 14.

The dynamic impingement depends primarily on drop size, liquid-water content, airspeed, and shape and size of the airship. The equation for dynamic impingement is

$$M_d = wVA_fE \tag{B3}$$

where the collection efficiency E is the fraction of drops in the path of the body that strike the surface. Calculated values of E are available for spheres and prolate ellipsoids of revolution of fineness ratios 5 and 10 (refs. 5 to 7). Since the portion of the ZPG airship envelope forward of the maximum-thickness point is very nearly an ellipsoid of fineness ratio 3.25, values of collection efficiency were obtained by interpolation. The results are shown in figure 15 in terms of drop size and airspeed. The values shown were determined for a 3000-foot altitude and -2° C and are applicable approximately from sea level to 5000 feet and from 0° to -10° C.

The liquid-water content may be eliminated from equation (B3) by introducing the rainfall rate and falling speed:

$$w = 5.2\ R/v$$

$$M_d = 5.2\ RA_f \frac{V}{v} E \tag{B4}$$

The ratio of the dynamic to the gravitational term is

$$\frac{M_d}{M_g} = \alpha = \frac{A_f}{A_h} \frac{V}{v} E \tag{B5}$$

and the total impingement is

$$M = M_d + M_g = 5.2\ RA_h\ (1 + \alpha) \tag{B6}$$

For the ZPG airship,

$$M = 1.02 \times 10^5\ R(1 + \alpha) \tag{B6a}$$

The falling speed of raindrops at 3000 feet is given as a function of drop diameter in figure 16 (based on refs. 8 and 9). Values of α for the ZPG airship, calculated from the data of figures 15 and 16, are presented in figure 17 as a function of drop diameter and airspeed.

The distribution of dynamic impingement as a function of the distance z measured along the axis from the nose was determined from the data of references 5 to 7. It was found that the local dynamic impingement rate in pounds per hour per axial foot is a linear function of z as given by

$$m_d = \frac{2M_d}{z_m} \left(1 - \frac{z}{z_m}\right) \tag{B7}$$

where z_m is the axial distance from the nose to the limit of dynamic impingement. Values of z_m obtained by interpolation from references 5

to 7 are shown in figure 18 as a function of drop diameter and airspeed. If the local dynamic impingement rate at the nose is divided by the rainfall rate, the result is

$$\frac{2M_d}{z_m R} = 2.04\times10^5 \frac{\alpha}{z_m} \tag{B8}$$

which represents the impingement on the nose in pounds per axial foot per inch of rain. This quantity is a function of airspeed and drop diameter and is shown in figure 19.

Figures 15, 17, 18, and 19 define impingement as a function of drop size and airspeed. For a given rainfall rate, the collection efficiency increases and the liquid-water content decreases with increasing drop size. As a result, the variation with drop size of total impingement is relatively small for drops greater than 0.6 millimeter in diameter. As shown in figure 17, the quantity $(1 + \alpha)$ changes by only 9 percent at 30 knots and 11.5 percent at 50 knots for a change in drop diameter from 0.6 to 1.8 millimeters. For this reason, no serious errors are introduced by using a statistical average relation between rainfall rate and drop diameter to express the impingement in terms of rainfall rate and airspeed. This relation, shown in figure 20, was derived from an empirical equation relating rainfall rate and liquid-water content from reference 10.

The elimination of drop size as an independent variable gives the following impingement results for the ZPG airship:

(1) Total impingement (lb/hr) as a function of airspeed and rainfall rate (fig. 21) (The gravitational impingement alone is shown by the curve for zero airspeed.)

(2) The local dynamic impingement rate at the nose (lb/(hr)(axial ft)) as a function of airspeed and rainfall rate (fig. 22)

(3) The limit of the dynamic impingement zone (ft from nose along axis) as a function of airspeed and rainfall rate (fig. 23)

The distribution of total impingement along the axis may be found by adding the local gravitational impingement, from figure 14, to the local dynamic impingement, obtained from equation (B7) using z_m from figure 23 and $2M_d/z_m$ from figure 22.

A convenient rule for estimating the total impingement rate which gives results within 5 percent of the values shown in figure 21 is as follows: The total impingement in thousands of pounds per hour is equal to the rainfall rate in hundredths of an inch per hour increased by 1 percent for each knot of airspeed in excess of 10 knots.

Effect of Heat Transfer on Icing Rates

In conditions of light freezing rain at temperatures considerably below freezing, all the water impinging on the airship freezes. Thus, the rate and distribution of icing are the same as the rate and distribution of impingement. As the water freezes, the liberated heat of fusion causes the surface temperature to rise above the air temperature until the rate of heat loss from the surface by convection and evaporation balances the rate of liberation of latent heat. At higher rates of water impingement the surface temperature may reach 32° F. Additional increases in impingement cannot increase the surface temperature above 32° F and therefore do not increase the evaporation and convection heat losses. The increase in ice formation due to an increase in impingement under these conditions is only enough to provide sufficient latent heat to raise the temperature of the additional impinging water to 32° F. The remainder of the additional water runs off in the liquid state. For any particular combination of airspeed, altitude, temperature, humidity, and position on the airship, there exists a critical rate of water impingement which is just sufficient to maintain the surface temperature at 32° F. The rate of ice formation per unit area under these conditions is the critical freezing rate f_{cr}.

Under these conditions, the rate of heat loss from the surface by convection $q_{as,c}$, and evaporation $q_{as,e}$, is balanced by the rate of production of heat by freezing $q_{as,fr}$. The rate of heat loss by radiation is much smaller than the convection term and is therefore neglected. Also neglected is transfer of heat into or out of the underlying surface. The convection term is:

$$q_{as,c} = H\left(32 - t_0 - \frac{rU_0^2}{2Jc_p}\right) \tag{B9}$$

The evaporation term $q_{as,e}$ is written to include the entire heat loss due to the change of enthalpy of the water that evaporates; the initial temperature of the rain drops is assumed to be the wet-bulb temperature:

$$q_{as,e} = \frac{H}{c_p}\frac{0.622\ (p_{32} - p_0)}{P}\left(h_{v,32} - h_{l,w} - \frac{U_0^2}{2J}\right) \tag{B10}$$

The rate of gain of heat due to the change of enthalpy of the water that freezes is

$$q_{as,fr} = f_{cr}\left(h_{l,w} + \frac{U_0^2}{2J} - h_{i,32}\right) \tag{B11}$$

Use of the kinetic wet-bulb temperature t_{kw} as a reference temperature is desirable because it makes the results applicable to unsaturated as well as saturated ambient conditions. The kinetic wet-bulb temperature is defined as the equilibrium temperature of a wet-bulb thermometer in a moving airstream when the wet bulb is covered with liquid water. When the airship is flying in clouds, the reading of a dry-bulb thermometer shielded from direct droplet impingement may be used as t_{kw}. When in clear air at temperatures below freezing, the wet-bulb thermometer yields the kinetic iced-bulb temperature t_{ki}, because the bulb is coated with ice instead of liquid water. The corrections shown in figure 24 may be used to obtain t_{kw} from t_{ki} and the relative humidity.

Equations (B10) and (B11) may be simplified by using the following approximation:

$$h_{l,w} + \frac{U_0^2}{2J} = h_{l,kw}$$

The kinetic temperature rise of the water drops is about half the wet-bulb kinetic temperature rise, and both are less than 1° F at speeds up to 60 knots. Thus, the error in the approximation is small compared with the enthalpy changes in evaporation (eq. (B10)) and freezing (eq. (B11)). With this simplification, the terms are substituted in the heat-balance equation $q_{as,c} + q_{as,e} = q_{as,fr}$, and the result is solved for f_{cr}:

$$f_{cr} = \frac{H}{(h_{l,kw} - h_{i,32})}\left[32 - t_0 - \frac{rU_0^2}{2Jc_p} + \frac{0.622}{c_p}\frac{(p_{32} - p_0)}{P}(h_{v,32} - h_{l,kw})\right] \tag{B12}$$

The psychrometric equation defining the kinetic wet-bulb temperature with respect to liquid water is

$$t_{kw} = t_0 + \frac{rU_0^2}{2Jc_p} - \frac{0.622}{c_p}\frac{(p_{kw} - p_0)}{P}(h_{v,kw} - h_{l,kw}) \tag{B13}$$

Combining equations (B12) and (B13) and rearranging the vapor-pressure - enthalpy products give

$$f_{cr} = \frac{H}{h_{l,kw} - h_{i,32}}\left\{32 - t_{kw} + \frac{0.622}{Pc_p}\left[(p_{32} - p_{kw})(h_{v,32} - h_{l,kw}) + (p_0 - p_{kw})(h_{v,kw} - h_{v,32})\right]\right\} \tag{B14}$$

Since $(p_0 - p_{kw})$ is less than $(p_{32} - p_{kw})$ and $(h_{v,kw} - h_{v,32})$ is less than 0.5 percent of $(h_{v,32} - h_{l,kw})$ for $32 > t_{kw} > 20$, the product $(p_0 - p_{kw})(h_{v,kw} - h_{v,32})$ can be neglected in equation (B14); hence,

$$f_{cr} = \frac{H}{h_{l,kw} - h_{i,32}}\left[32 - t_{kw} + \frac{0.622}{Pc_p}(p_{32} - p_{kw})(h_{v,32} - h_{l,kw})\right] \quad (B15)$$

This relation gives the critical freezing rate in terms of the local heat-transfer coefficient and the kinetic wet-bulb temperature. Because of the large size of an airship, the boundary layer is turbulent at ordinary flight speeds except for a very small area at the nose. The heat-transfer coefficient is given by the following equation, which gives good agreement with experimental data for blunt bodies of revolution in turbulent flow (ref. 11):

$$Nu = \frac{Hs}{k} = 0.0296\ Pr^{1/3}\ Re^{0.8} \quad (B16)$$

which gives

$$H = 0.0296\ k\ Pr^{1/3}\ (\rho/\mu)^{0.8}\ U_s^{0.8}\ s^{-0.2} \quad (B17)$$

With $U_s^{0.8} = (U_s/U_0)^{0.8}(1.689\ V)^{0.8} = 1.521\ (U_s/U_0)^{0.8}V^{0.8}$, substitution in equation (B15) gives

$$f_{cr} = \Phi(U_s/U_0)^{0.8}\ V^{0.8}/s^{0.2} \quad (B18)$$

where

$$\Phi = \frac{0.0450\ kPr^{1/3}(\rho/\mu)^{0.8}}{h_{l,kw} - h_{i,32}}\left[32 - t_{kw} + \frac{0.622}{Pc_p}(p_{32} - p_{kw})(h_{v,32} - h_{l,kw})\right] \quad (B19)$$

is a function of altitude and kinetic wet-bulb temperature. Values of Φ were calculated for a range of pressure altitudes from 1000 to 5000 feet and t_{kw} from 32° to 16° F. The quantity $kPr^{1/3}\ (\rho/\mu)^{0.8}$ was evaluated at t_{kw}. Values of U_s/U_0 were calculated from surface-velocity data for an ellipsoidal body from reference 11.

It was found that Φ could be represented within ±0.5 percent over this range of pressure altitude and temperature (1000 to 5000 ft and 16° to 32° F) by the following approximation

$$\Phi = (0.0080\ \theta + 0.000025\ \theta^2)(1 - 0.0000143\ Z_p) \qquad \text{(B20)}$$

where $\theta = 32 - t_{kw}$ is the depression below freezing of the kinetic wet-bulb temperature.

Over a limited range of temperature from 32° F to about 20° F, Φ is almost a linear function of θ. For convenience and simplicity in the application of critical-icing-rate calculations, the following linear approximation was used in the calculations presented in this report:

$$\Phi = 0.0082\ \theta\ (1 - 0.0000143\ Z_p) \qquad \text{(B21)}$$

For altitudes between 1000 and 5000 feet, the error arising from using equation (B21) instead of equation (B19) is approximately 1 percent at $\theta = 4$, 0 at $\theta = 8$, -1.3 percent at $\theta = 12$, and -2.8 percent at $\theta = 16$. Combining equations (B21) and (B18) gives the final expression for the critical freezing rate per unit area:

$$f_{cr} = 0.0082\ \theta\ (1 - 0.0000143\ Z_p)(U_s/U_0)^{0.8}\ V^{0.8}/s^{0.2}$$

The critical freezing rate per unit distance along the axis of the airship is given by

$$F_{cr} = f_{cr} \pi D_z \frac{\lambda}{2} \frac{ds}{dz}$$

where λ is the wetted-area factor. In the region next to the nose, where the envelope is wetted all the way around, $\lambda = 2$; aft of the dynamic impingement area, where the top half only is wetted, $\lambda = 1$. The transition from $\lambda = 2$ to $\lambda = 1$ occurs over a small range of z, just forward of z_m.

APPENDIX C

CALCULATION OF OFFSHORE HEATING OF COLD AIR

It is required to calculate the time rate of increase of temperature T_o at the base of a cold-air layer of depth Z_{ib} flowing over a relatively warm water surface. The bottom of the layer ($Z = 0$) is taken as outside the boundary layer at about 8 meters above the sea surface. "Surface" temperature and wind speed refer to this height. It is assumed that the cold-air layer is thoroughly mixed at all times and thus has constant total water mixing ratio x_t throughout, a dry adiabatic lapse rate up to the condensation level Z_{cond}, and a saturated adiabatic lapse rate from Z_{cond} to Z_{ib}. If the dry adiabatic line is extended from

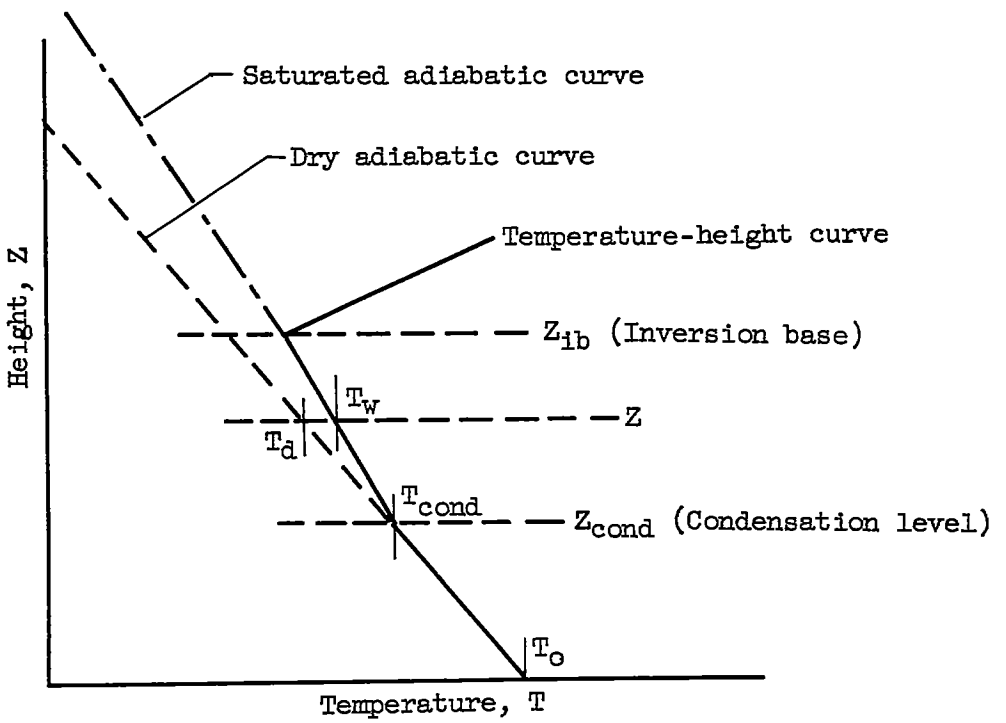

Z_{cond} to Z_{ib}, the temperature represented by a point on this line at height Z is the dry adiabatic temperature T_d. The corresponding temperature T_w on the saturated adiabatic line is greater than T_d because of the latent heat released by condensation of liquid water:

$$T_w = T_d + \frac{Q_v}{c_p} x_l \tag{C1}$$

Since this analysis applies to temperatures near and below freezing, the total water mixing ratio $x_t = x_l + x_v$ is always less than about 0.005. Thus, the specific heat and density of the mixture of air, vapor, and liquid water may be taken as approximately equal to those of air at the same pressure and temperature.

When heat and water vapor are introduced and mixed throughout the layer, the time rate of increase in enthalpy per unit horizontal area is

$$q_a = \int_0^{Z_{cond}} c_p\rho \left(\frac{dT_d}{d\tau}\right) dZ + \int_{Z_{cond}}^{Z_{ib}} c_p\rho \left(\frac{dT_w}{d\tau}\right) dZ + \int_0^{Z_{ib}} Q_v\rho \left(\frac{dx_v}{d\tau}\right) dZ \tag{C2}$$

From equation (C1)(for the interval Z_{cond} to Z_{ib})

$$\frac{dT_w}{d\tau} = \frac{dT_d}{d\tau} + \frac{Q_v}{c_p}\frac{dx_l}{d\tau}$$

and since $x_t = x_l + x_v$

$$q_a = \int_0^{Z_{ib}} c_p\rho \left(\frac{dT_d}{d\tau}\right) dZ + \int_0^{Z_{ib}} Q_v\rho \left(\frac{dx_t}{d\tau}\right) dZ \tag{C3}$$

Since the dry adiabatic lapse rate is constant, $dT_d/d\tau$ is independent of Z and equal to $dT_o/d\tau$ as long as $x_l = 0$ at $Z = 0$. Also, the total mixing ratio x_t is assumed independent of Z; therefore,

$$q_a = Z_{ib}\bar{\rho}\left(c_p \frac{dT_o}{d\tau} + Q_v \frac{dx_t}{d\tau}\right) \tag{C4}$$

The rate of enthalpy loss from the sea surface per unit area is the sum of a convection term,

$$q_{ss,c} = H_c(T_{ss} - T_o) \tag{C5}$$

an evaporation term,

$$q_{ss,e} = (H_c/c_p)\, Q_v(x_{v,sat} - x_t) \tag{C6}$$

and a radiation term,

$$q_{ss,r} = \sigma(T_{ss}^{*4} - T_{cond}^{*4}) = H_r(T_{ss} - T_{cond}) \tag{C7}$$

Equation (C7) is based on the assumption that the sea surface and the cloud base radiate essentially as black bodies at temperatures near 275° K.

The heat-balance equation is

$$q_a = q_{ss,c} + q_{ss,e} + q_{ss,r}$$

Thus,

$$Z_{ib}\overline{\rho}c_p\frac{dT_o}{d\tau} + Z_{ib}\overline{\rho}Q_v\frac{dx_t}{d\tau} = H_c(T_{ss} - T_o) + \frac{H_c}{c_p}Q_v(x_{v,sat} - x_t) + H_r(T_{ss} - T_{cond}) \tag{C8}$$

The rate of increase of water content in the cold-air layer equals the rate of evaporation from the surface; therefore,

$$Z_{ib}\overline{\rho}\frac{dx_t}{d\tau} = \frac{H_c}{c_p}(x_{v,sat} - x_t) \tag{C9}$$

Subtracting equation (C9) from equation (C8), dividing by $c_p\rho_o$, and introducing the wind speed $V = dy/d\tau$ give

$$Z_{ib}\frac{\overline{\rho}}{\rho_o}\frac{dT_o}{d\tau} = \frac{H_c}{c_p\rho_o V}(T_{ss} - T_o)\frac{dy}{d\tau} + \frac{H_r}{c_p\rho_o V}(T_{ss} - T_{cond})\frac{dy}{d\tau} \tag{C10}$$

Introducing the Stanton number $St \equiv H/18.53c_p\rho V$ (one knot = 18.53 hectometers/hr) and solving for dT_o/dy give

$$\frac{dT_o}{dy} = \frac{\rho_o}{\overline{\rho}}\frac{18.53}{Z_{ib}}\left[St_c(T_{ss} - T_o) + St_r(T_{ss} - T_{cond})\right] \tag{C11}$$

Use of this equation for numerical calculations requires values of the Stanton numbers for convection and radiation. The Stanton number for convection heat transfer was obtained from analyses of the turbulent transfer of water vapor at the sea surface (refs. 12 and 13). The principle of the similarity of heat and mass transfer in turbulent flow allows the calculation of the Stanton number from the evaporation coefficients. For a rough surface (V > 13 knots), the theoretical value of the Stanton number is 0.0031 based on a roughness length of 0.6 centimeter and a height of 8 meters for the measurement of surface temperature and wind. For a smooth surface, the theoretical value varies slightly with the wind speed but is close to an average of 0.0010 for winds from 4 to 13 knots. A study of average evaporation over world ocean areas (ref. 12) yields an empirical average evaporation coefficient corresponding

to a Stanton number of 0.0020, about midway between the theoretical values for rough and smooth surfaces. Evaporation coefficients calculated from vapor-pressure-gradient data given in reference 13 correspond to St_c values from 0.0004 to 0.0019 at winds less than 12 knots and St_c values from 0.0023 to 0.0034 at winds over 16 knots. The values of St_c used herein are the theoretical values. For $V < 13$ knots,

$$St_c = 0.0010$$

For $V > 13$ knots,

$$St_c = 0.0031$$

The Stanton number for radiation was calculated from equation (C7) using an average value of T^*_{cond} of about 271° K and $T^*_{ss} = 279°$ K. When V is in knots,

$$St_r = 0.0072/V$$

In order to apply equation (C11) to calculate the probable effect of a trajectory over water on a given freezing-rain air-mass structure, it is necessary to know the temperature as a function of height for the initial conditions when the air crosses the coast. The summary of temperature and freezing-level data in freezing rain referred to previously in the discussion of figure 9 includes a listing of the surface temperature $T_{o,cl}$ in °C and the height above the ground of the first freezing level Z_{fr} in hectometers. These two quantities were used to define an ideal temperature-height curve as follows. A lapse rate of 0.72° C per hectometer was assumed from the surface to a height of $1/2\ Z_{fr}$. A linear increase in temperature was assumed from this point to the freezing level at Z_{fr}. Comparison with actual soundings shown in figure 25 shows that the assumptions are realistic. This relation is expressed in the following equation, in which Z_{fr} and Z_{ib} are in hectometers and T_o and $T_{o,cl}$ in °C:

$$Z_{ib} = \frac{Z_{fr}}{2}\left(1 + \frac{T_o - T_{o,cl}}{0.72\ Z_{fr} - T_{o,cl}}\right) \qquad (C12)$$

The surface relative humidity in cold polar air at sea is generally from 70 to 80 percent (ref. 14), corresponding to a condensation level of about 400 meters. Thus, a constant value of 4° C was assumed for $T_o - T_{cond}$. A constant value of 6° C was chosen for T_{ss}, as representing January conditions offshore at the latitude of Boston (ref. 15).

The value of Z_{ib} from equation (C12) and the values $T_{ss} = 6$ and $T_{cond} = T_o - 4$ were substituted in equation (C11), and the result was

integrated with respect to T_o, in order to determine the distance offshore y (nautical miles) at which T_o attains a particular value $T_{o,y}$

$$y = \frac{Z_{fr}}{37.06\ b}\frac{\bar{\rho}}{\rho_o}\left[\left(c + \frac{a}{b}\right)\ln\left(\frac{a - bT_{o,cl}}{a - bT_{o,y}}\right) - (T_{o,y} - T_{o,cl})\right] \quad (C13)$$

where

$$a = (0.72\ Z_{fr} - T_{o,cl})(6\ St_c + 10\ St_r)$$

$$b = (0.72\ Z_{fr} - T_{o,cl})(St_c + St_r)$$

$$c = 0.72\ Z_{fr} - 2T_{o,cl}$$

In figure 26 is shown the calculated distance offshore y at which the surface-air temperature reaches 2° C for winds of 5, 10, and 20 knots. The distance y is given as a function of the initial surface-air temperature at the coast $T_{o,cl}$ and the height of the freezing level Z_{fr} assuming the sea-surface temperature is 6° C. The numbers between the curves in figure 26 are numbers of observations of temperature and freezing level (measured over land) in the intervals indicated. The variation of offshore heating with wind speed is a result of the variation of St_c and St_r. The convection heat transfer per mile increases by a factor of about 3 at the critical wind speed (about 13 knots) when the surface changes from smooth to rough. The heat loss from the sea per hour by radiation is independent of wind; therefore, the radiation transfer per mile varies inversely with the wind speed. Thus, the total heating per mile approaches a maximum at very low wind speeds with radiation predominant. At winds just below 13 knots the heating per mile is a minimum with convection accounting for about two-thirds of the total. At winds over 13 knots, convection heating per mile is constant at a relatively high value, while the radiation effect slowly approaches zero with increasing wind.

In the absence of actual data on wind frequencies, it was assumed that the median wind speed is about 13 knots, with half the cases represented by the results calculated for 20 knots and the other half equally divided between 5 and 10 knots. Thus, the frequencies in figure 26 were weighted in the ratio 1:1:2 for winds of 5, 10, and 20 knots and combined in figure 13 to show the percentage of cases of freezing rain that would be eliminated by heating to 2° C as a function of length of trajectory over water at 6° C.

APPENDIX D

DERIVATION OF RAINFALL FREQUENCY DISTRIBUTION APPLICABLE TO FREEZING RAIN

The frequency distribution of rainfall rate in freezing rain is difficult to establish because statistics on rainfall rate as ordinarily presented do not include simultaneous data on temperature and state (solid or liquid) of the water particles. From theoretical considerations it is known that, for a given amount of lifting, the intensity of precipitation depends on the moisture content, and thus also on the temperature of the air that is being lifted. Rainfall rates therefore increase on the average with increasing temperature of the air mass in which the rain is formed. In the case of freezing rain, the temperature of the base of the warm air mass in which the rain is formed, is usually just a few degrees above freezing regardless of the cold-air-mass temperature. Thus, a reasonable estimate of the rainfall intensity distribution in freezing rain may be obtained from the distribution of ordinary rain intensity in the temperature range from about 32° to 45° F, and this rainfall distribution may be assumed to be independent of the temperature in the cold-air layer.

The climatological data published by the U.S. Weather Bureau (refs. 16 and 17) contain hourly precipitation totals and daily maximum and minimum temperatures. The desired rain intensity distribution was obtained by selecting days on which precipitation was general in New England and tabulating the hourly precipitation amounts recorded at stations having minimum temperatures of 32° F or higher and maximum temperatures of 45° F or lower. The resulting rainfall frequency distribution is shown in figure 11.

REFERENCES

1. Hillendahl, Wesley H.: A Flight Investigation of the Ice-Prevention Requirements of the United States Naval K-Type Airships. NACA WR A-4, 1945. (Supersedes NACA MR A5J19a.)

2. Perkins, Porter J., and Kline, Dwight B.: Analysis of Meteorological Data Obtained During Flight in a Supercooled Stratiform Cloud of High Liquid-Water Content. NACA RM E51D18, 1951.

3. Hardy, J. K.: An Analysis of the Dissipation of Heat in Conditions of Icing from a Section of the Wing of the C-46 Airplane. NACA Rep. 831, 1945. (Supersedes NACA ARR 4I11a.)

4. Ludlam, F. H.: The Heat Economy of a Rimed Cylinder. Quarterly Jour. Roy. Meteorological Soc., vol. 77, no. 334, Oct. 1951, pp. 663-666.

5. Dorsch, Robert G., Saper, Paul G., and Kadow, Charles F.: Impingement of Water Droplets on a Sphere. NACA TN 3587, 1955.

6. Dorsch, Robert G., Brun, Rinaldo J., and Gregg, John L.: Impingement of Water Droplets on an Ellipsoid with Fineness Ratio 5 in Axisymmetric Flow. NACA TN 3099, 1954.

7. Brun, Rinaldo J., and Dorsch, Robert G.: Impingement of Water Droplets on an Ellipsoid with Fineness Ratio 10 in Axisymmetric Flow. NACA TN 3147, 1954.

8. Gunn, Ross, and Kinzer, Gilbert D.: The Terminal Velocity of Fall for Water Droplets in Stagnant Air. Jour. Meteorology, vol. 6, no. 4, Aug. 1949, pp. 243-248.

9. Best, A. C.: Emperical Formulae for the Terminal Velocity of Water Drops Falling Through the Atmosphere. Quarterly Jour. Roy. Meteorological Soc., vol. 76, no. 329, July 1950, pp. 302-311.

10. Marshall, J. S., Langille, R. C., and Palmer, W. McK.: Measurement of Rainfall by Radar. Jour. Meteorology, vol. 4, no. 6, Dec. 1947, pp. 186-192.

11. Lewis, James P., and Ruggeri, Robert S.: Investigation of Heat Transfer from a Stationary and Rotating Ellipsoidal Forebody of Fineness Ratio 3. NACA TN 3837, 1956.

12. Jacobs, Woodrow C.: Large-Scale Aspects of Energy Transformation Over the Oceans. Compendium of Meteorology, Am. Meteorological Soc., 1951, pp. 1057-1070.

13. Sverdrup, H. U.: Evaporation from the Oceans. Compendium of Meteorology, Am. Meteorological Soc., 1951, pp. 1071-1081.

14. Sverdrup, H. U.: Oceanography. Handbook of Meteorology, McGraw-Hill Book Co., Inc., 1945, pp. 1031-1056.

15. McDonald, Willard F.: Atlas of Climatic Charts of the Oceans. W.B. No. 1247, Weather Bur., U.S. Dept. Agriculture, 1938.

16. Anon.: Hourly Precipitation Data (New England). Weather Bur., U.S. Dept. Commerce, vols. 5-7, 1955-1957.

17. Anon.: Climatological Data (New England). Weather Bur., U.S. Dept. Commerce, LXVIII-LXX, 1955-57.

TABLE I. - DATA FROM ZPG-2 AIRSHIP ICING FLIGHTS

Flight	Icing encounter	Date of flight	Time of icing	Duration of icing, min	Average rate of ice accretion, in./hr	Total ice accumulation, in.	Average liquid-water content, g/cu m	Droplet diameter, microns	Outside air temperature, °C	Pressure altitude, ft	Average true airspeed, knots	Estimated ice load, lb	Type of ice	Geographic location during icing	Remarks
1	-	Jan. 25, 1955	1:18 to 1:58 p. m.	40	0.67	0.45	0.33	—	-6.0	4400	47	----	Glaze and rime	Vicinity of Nantucket Island	Oscillating antennas
2	-	Nov. 8, 1955	3:05 to 3:26 p. m.	20	1.10	0.37	0.54	—	-6.0	5600	47	----	Rime	Vicinity of Concord, N. H.	----------
3	-	Dec. 4, 1955	9:50 to 10:59 a. m.	69	0.84	1.08	0.45	--	-1.5	3000	48	4000	Glaze (freezing drizzle)	South Weymouth	Severe car vibration
4	-	Jan. 3, 1956	10:00 to 10:30 a. m.	[a]30	-----	-----	----	—	0	2000	45	----	Glaze (freezing rain)	South Weymouth	----------
5	a	Jan. 15, 1956	9:48 to 10:44 a. m.	42	0.31	0.22	0.20	—	-1.5	2400	55	----	Glaze (freezing drizzle)	South Weymouth	Slight car vibration
	b		12:37 to 1:45 p. m.	41	.59	.40	.35	--	-2.0	2400	58	----	Glaze	Cape Cod area	Excessive car vibration
	c		2:40 to 3:52 p. m.	43	.27	.19	.15	--	-1.0	2900	42	----	Glaze	South Weymouth	Control-system failure after flight
6	-	Feb. 10, 1956	----------	69	0.86	0.78	0.34	--	-1.5	3000	44	----	Rime	----------	Control-system difficulty
7	-	Dec. 27, 1956	7:30 to 7:52 a. m.	22	0.91	0.34	0.42	9	-2.5	3500	50	----	Rime	Between South Weymouth and Cape Cod	----------
8	a	Jan. 15, 1957	5:30 to 6:50 a. m.	[a]180	[a]0.17	[a]0.50	----	--	-10.0	2980	47	2000	Rime	10-Day barrier station	Prolonged rime icing encounters
	b		2:30 to 5:10 p. m.	[a]40	.15	[a].10	----	--	-8.5	2800	41				
	c		4:40 to 5:10 p. m.	[a]30	.15	[a].08	0.08	8	-9.0	3000	38				
	d		11:20 to 12:00 p. m.	[a]40	.75 to 1.00	[a].60	----	--	-2.5	2900	42				
9	-	Jan. 16, 1957	6:10 to 6:33 p. m.	23	0.29	0.11	0.15	19	-1.0	3000	34	500	Rime	Between South Weymouth and barrier station	Snow load on takeoff

[a]Estimated value.

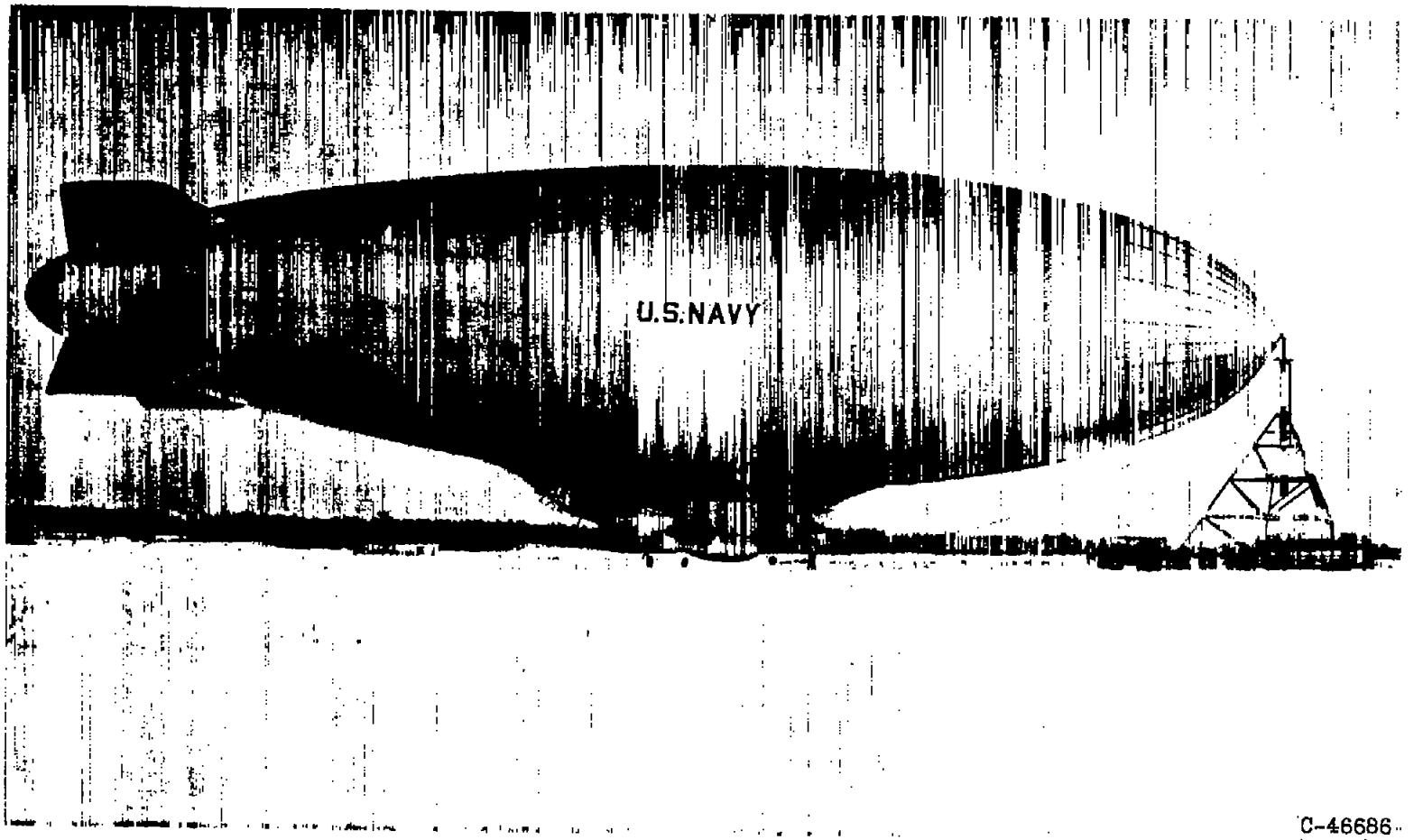

Figure 1. - Side view of ZPG airship. (Obtained from U.S. Navy.)

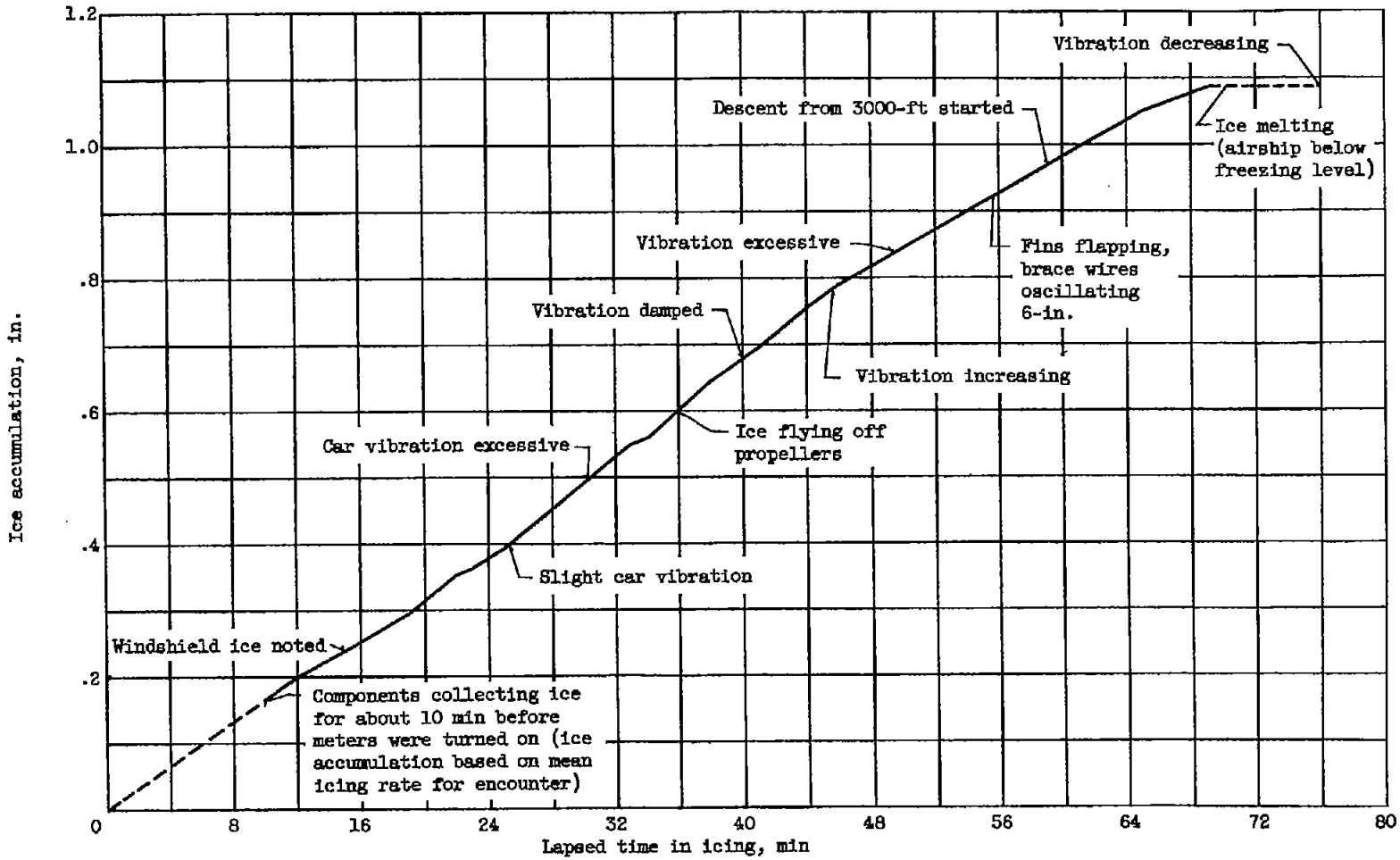

Figure 2. - Measured ice accumulation and associated effects occurring during test flight number 3.

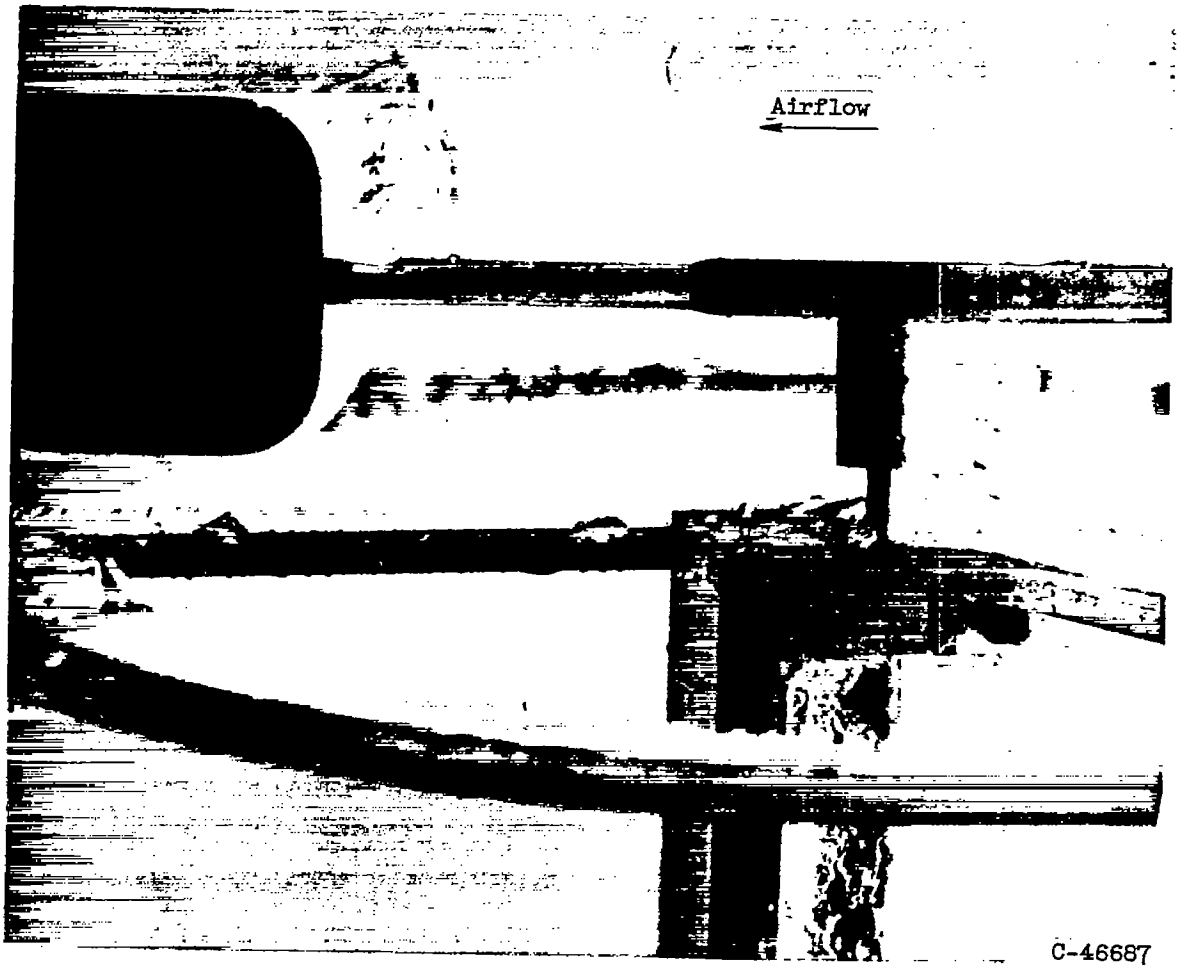

(a) Clear ice formed during flight number 3 in freezing drizzle.

Figure 3. - In-flight photographs of exposed yawmeter showing ice accretions formed under freezing-drizzle and rime-ice conditions. (Obtained from U.S. Navy.)

(b) Rime-ice formed during flight number 8.

Figure 3. - Concluded. In-flight photographs of exposed yawmeter showing ice accretions formed under freezing-drizzle and rime-ice conditions. (Obtained from U.S. Navy.)

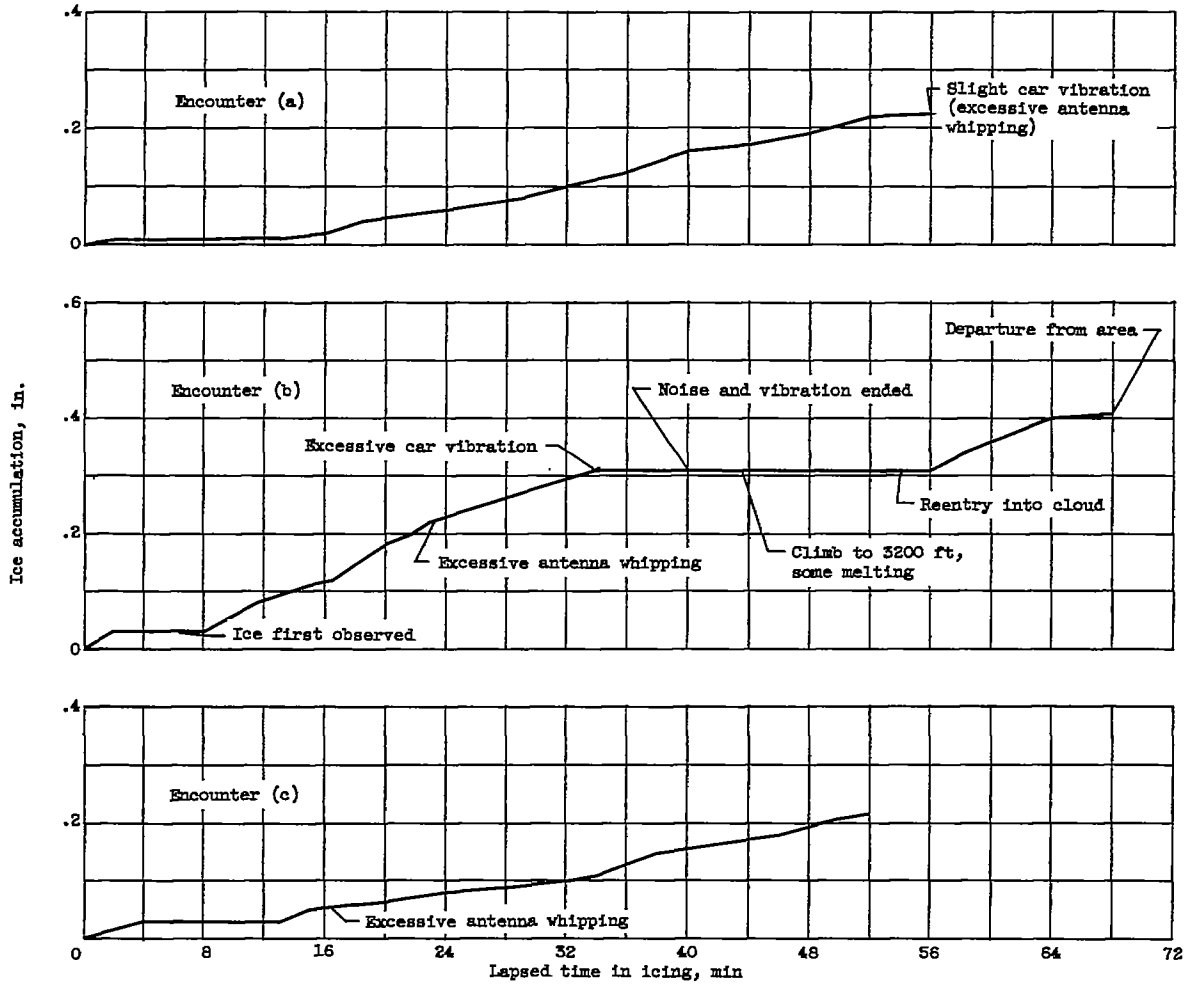

Figure 4. - Measured ice accumulation and associated effects occurring during test flight number 5.

(a) Snow distributed along top of envelope following 2-hour flight in light to moderate snow at -2° to -6° C.

Figure 5. - Location of snow catch observed on airship envelope. (Obtained from U.S. Navy.)

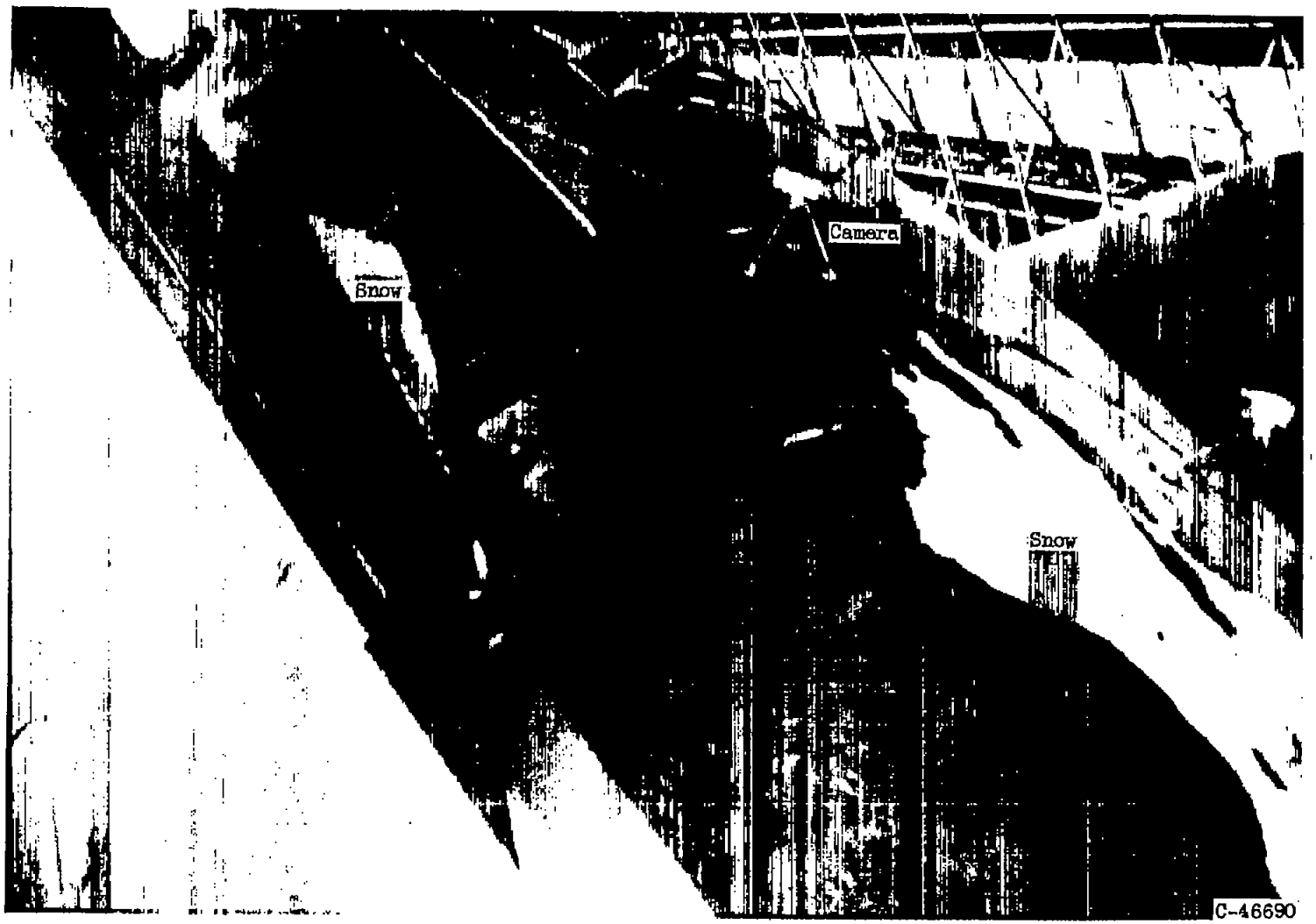

(b) Snow in aft area between top fins following two 40-hour flights.

Figure 5. - Concluded. Location of snow catch observed on airship envelope. (Obtained from U.S. Navy.)

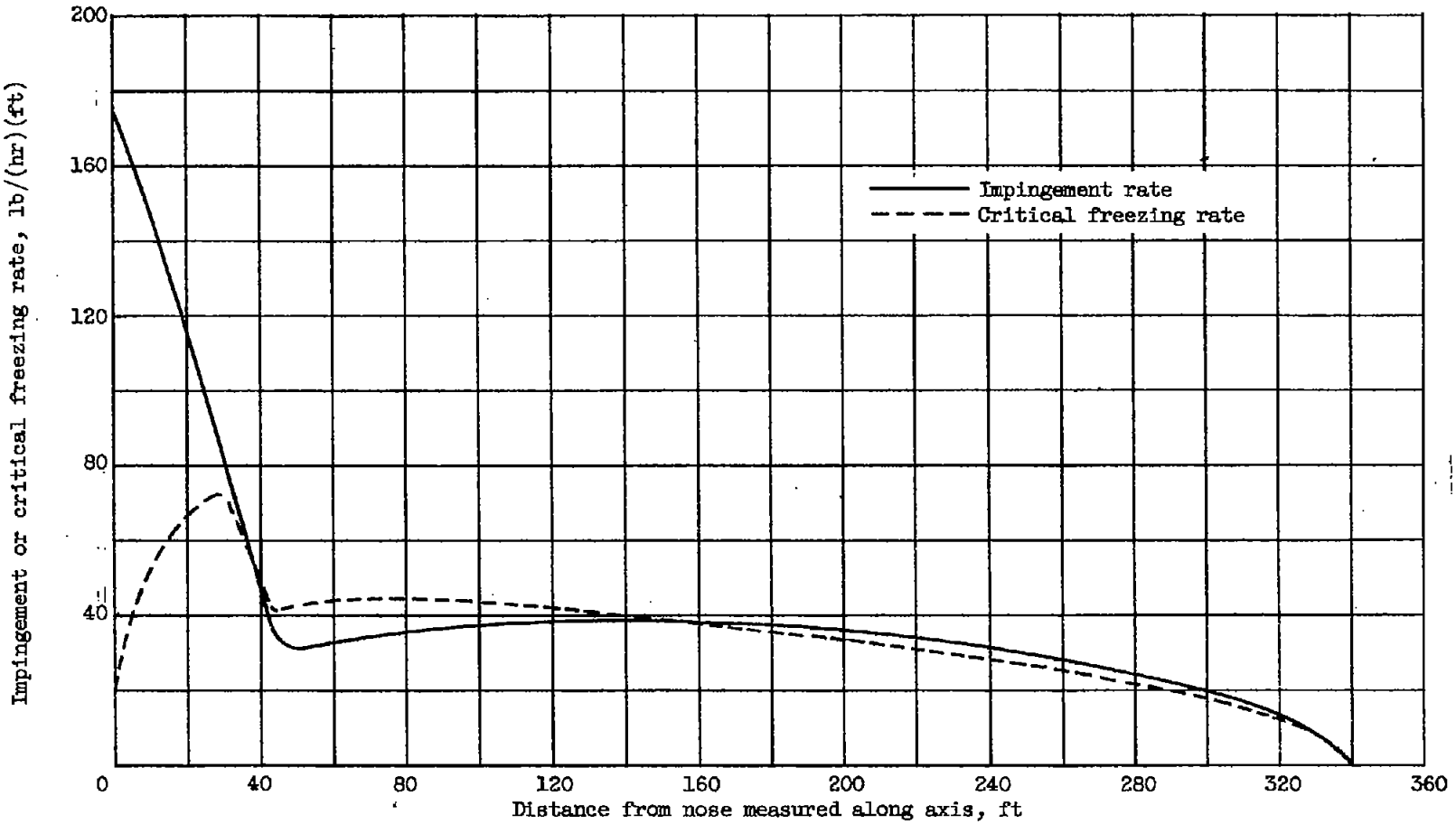

(a) Conditions of partial runoff. Rainfall rate, 0.10 inch per hour; airspeed, 50 knots; kinetic wet-bulb temperature, 27° F.

Figure 6. - Comparison of critical freezing and impingement rates. Pressure altitude, 3000 feet.

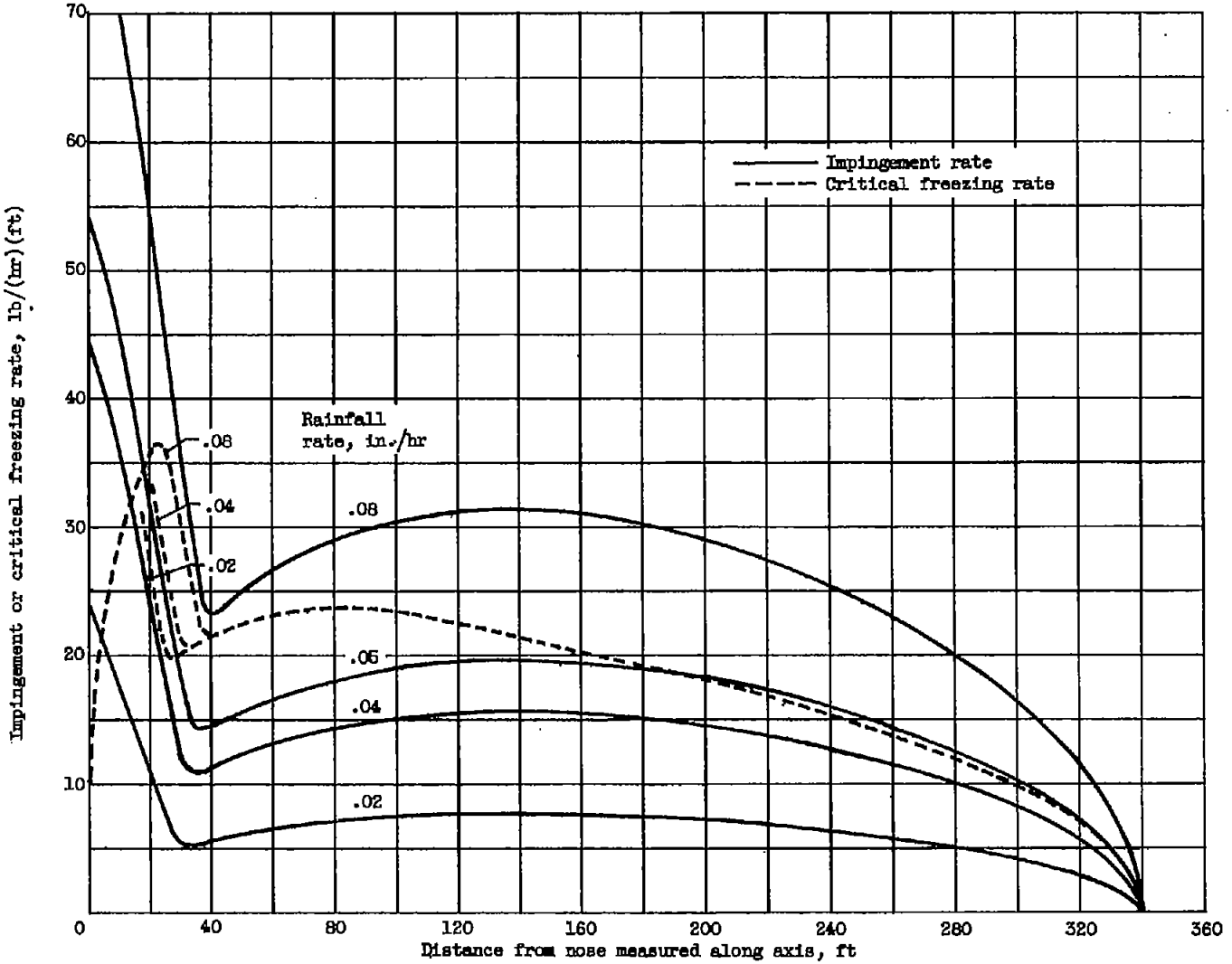

(b) Comparison for range of rainfall rates. Airspeed, 30 knots; kinetic wet-bulb temperature, 28° F.

Figure 6. - Concluded. Comparison of critical freezing and impingement rates. Pressure altitude, 3000 feet.

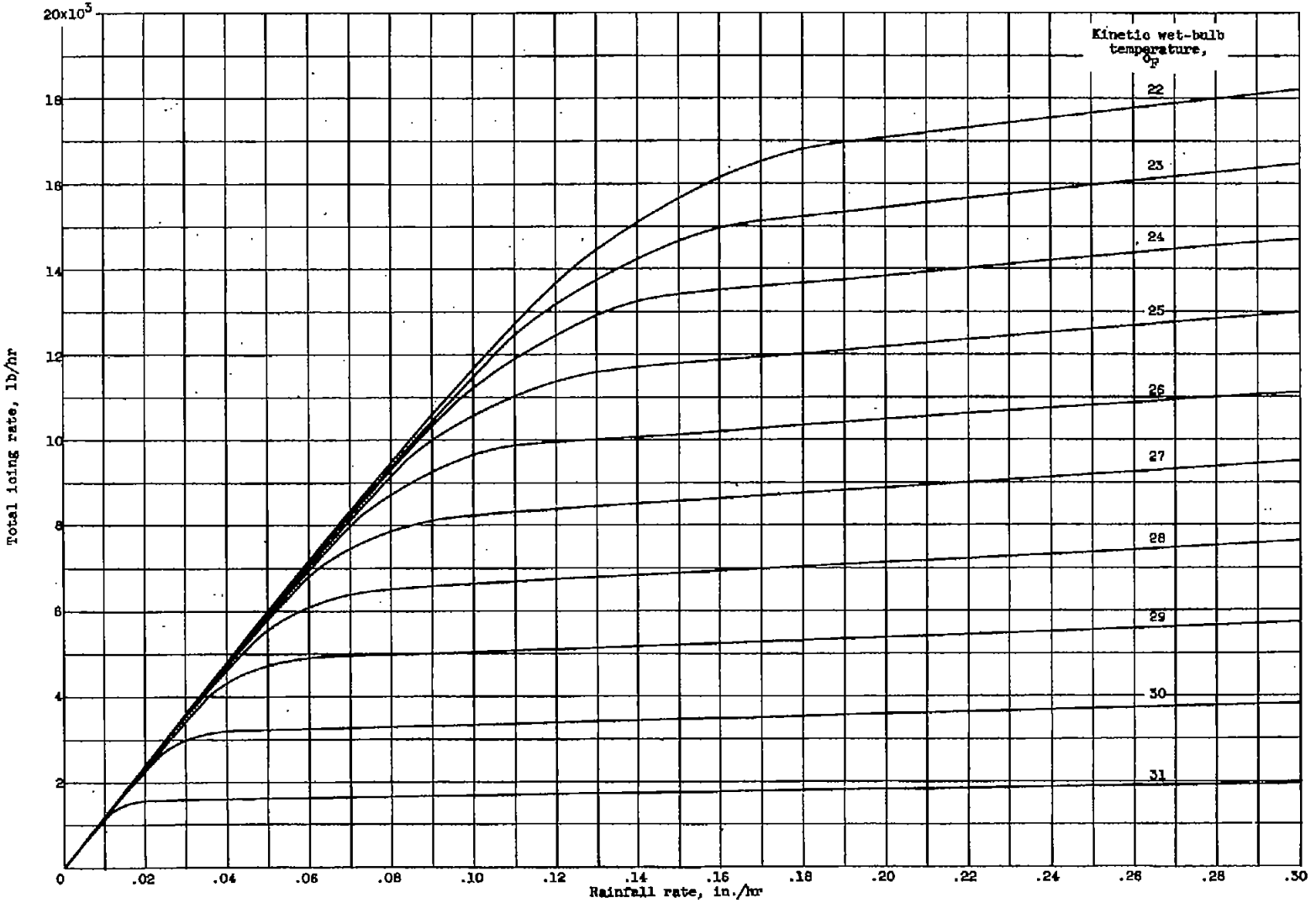

(a) Airspeed, 30 knots.

Figure 7. - Icing rate as function of rainfall rate for various temperatures. Pressure altitude, 3000 feet.

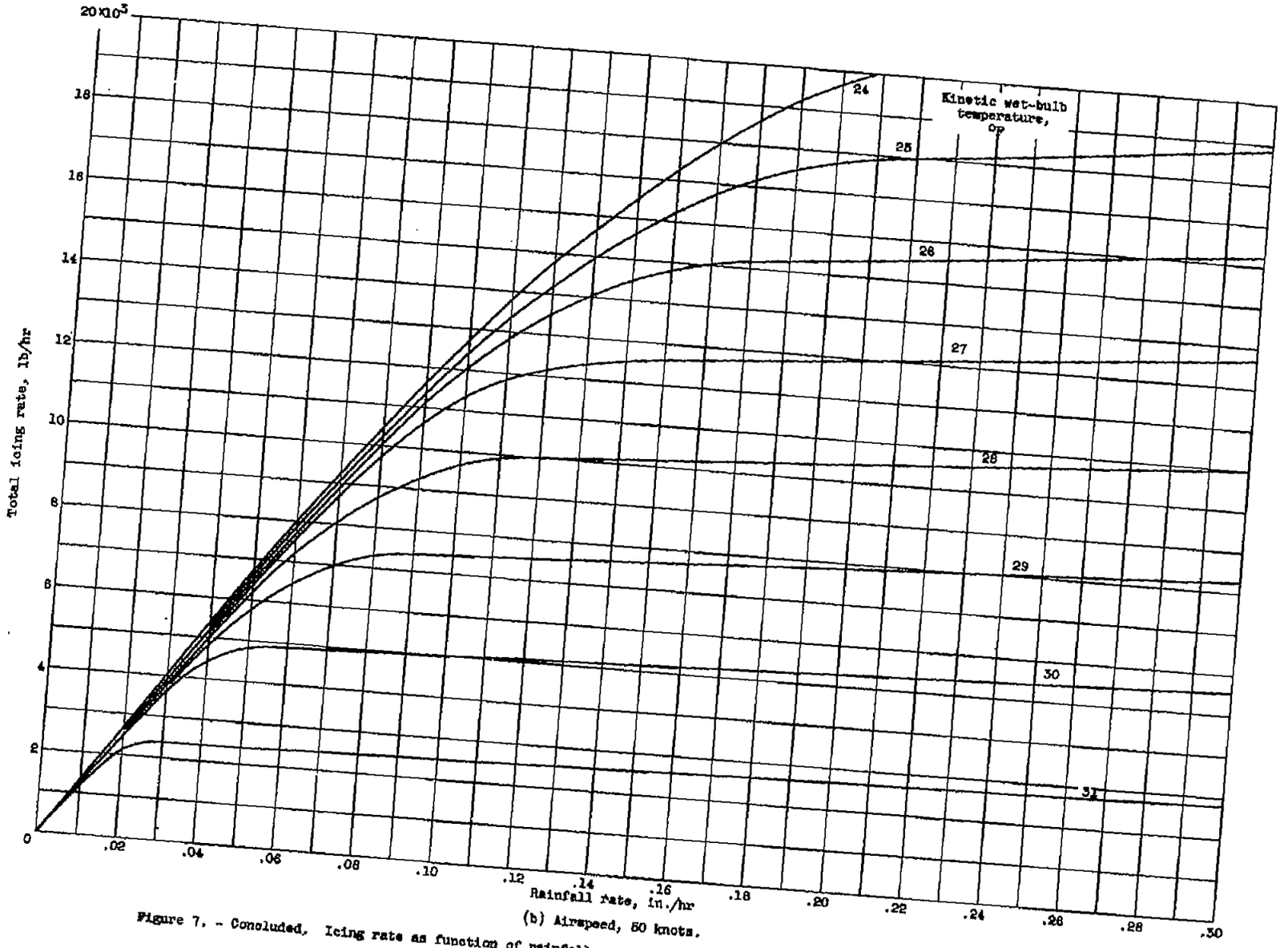

(b) Airspeed, 50 knots.

Figure 7. - Concluded. Icing rate as function of rainfall rate for various temperatures. Pressure altitude, 3000 feet.

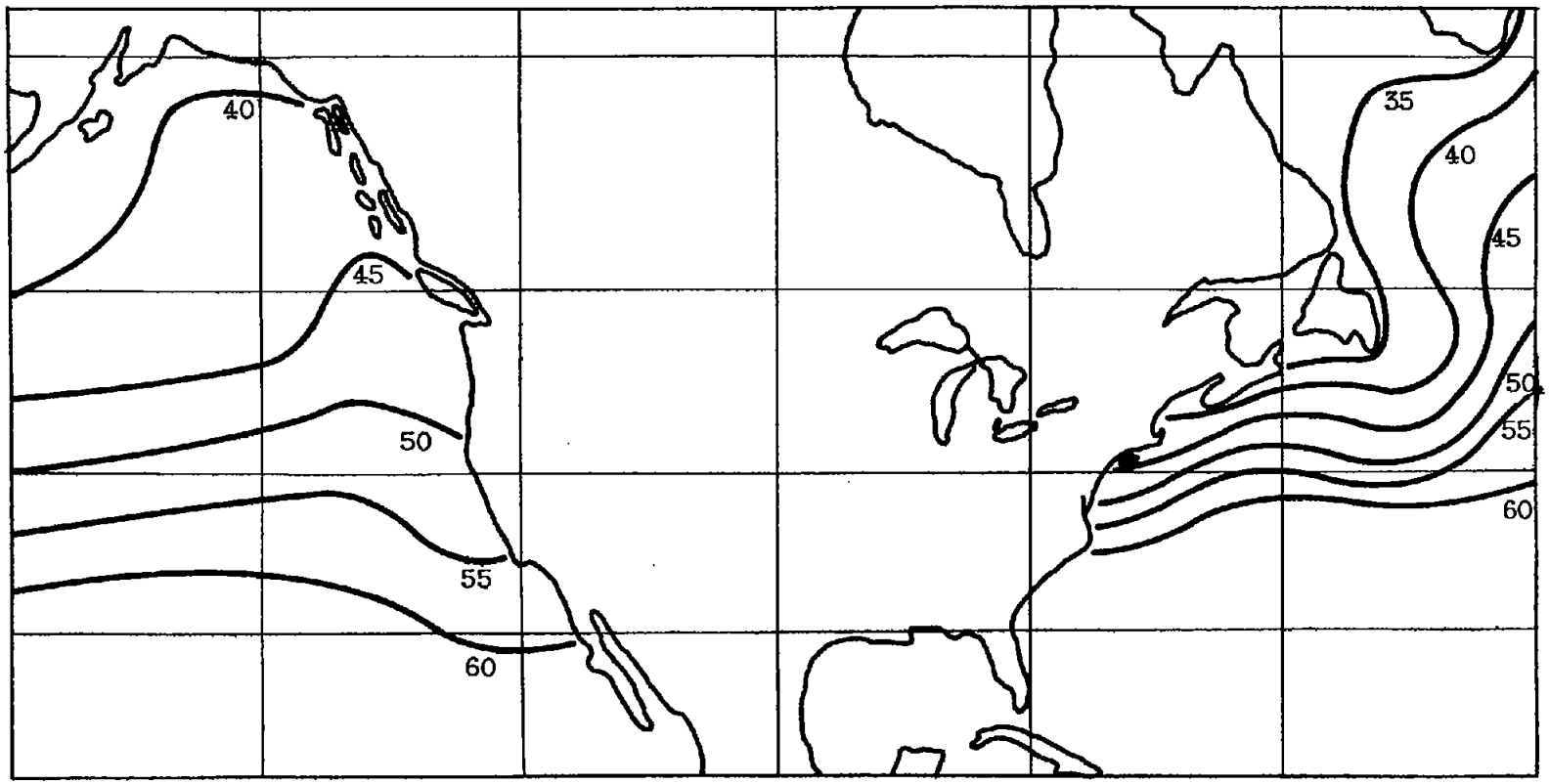

Figure 8. - Average January sea-surface temperatures (^{o}F) near coasts of North America. (Based on data from ref. 15.)

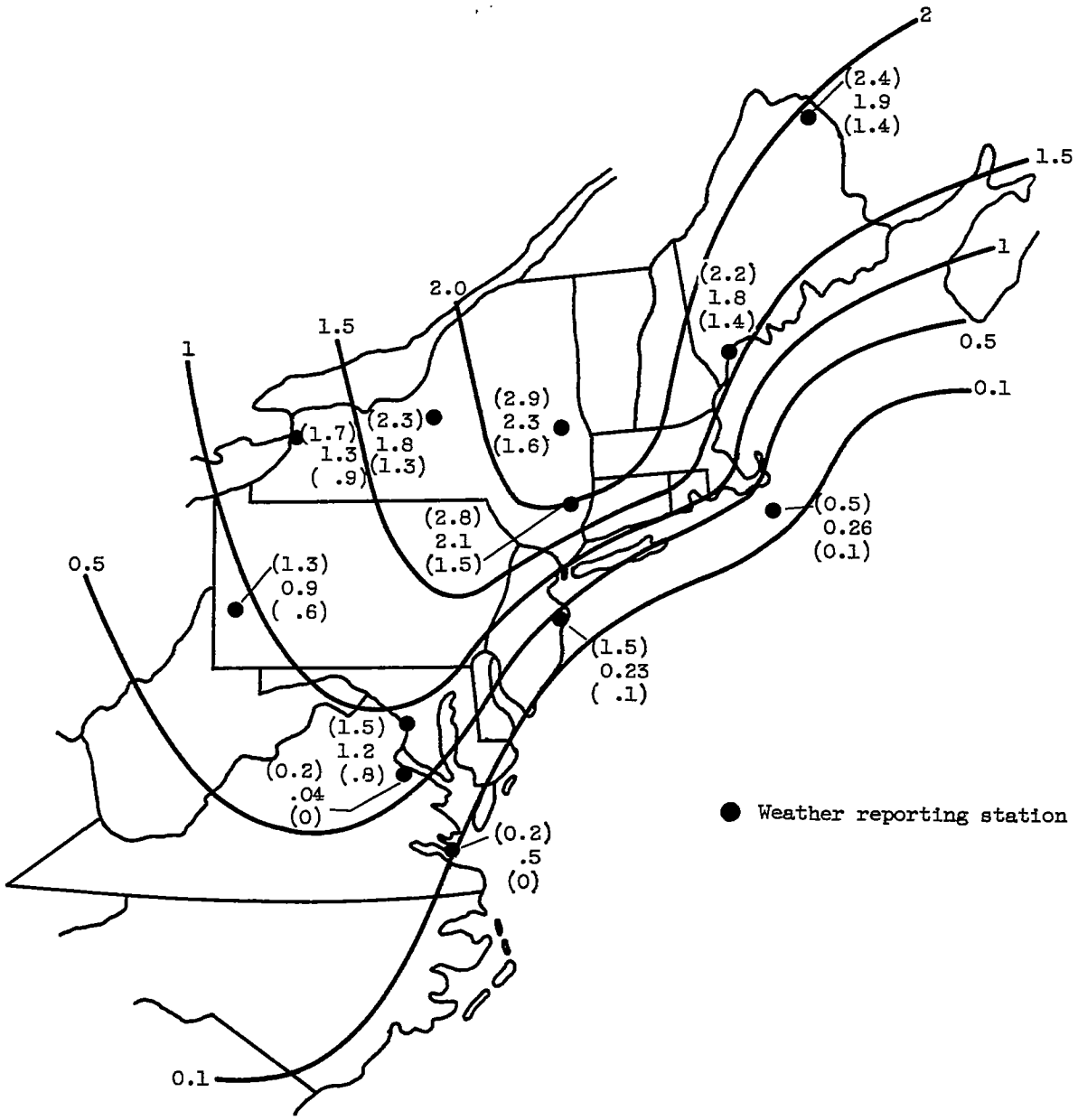

Figure 9. - Percentage of observations in northeastern United States in which freezing rain was reported. Averages for December, January, and February based on two daily observations for periods of 7 to 14 years. Limits of 90 percent confidence band shown in parentheses.

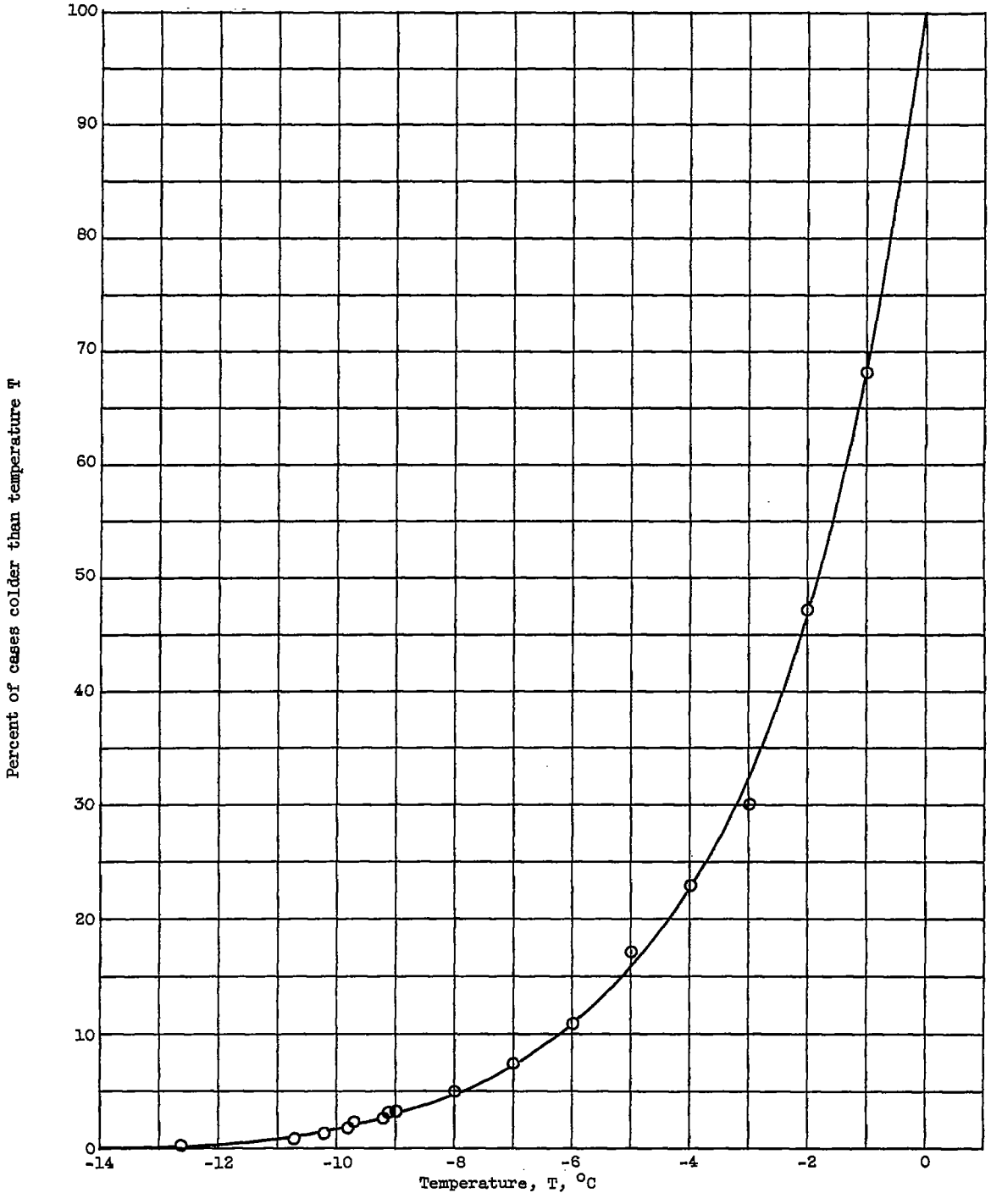

Figure 10. - Frequency distribution of surface-air temperature in freezing rain at selected stations in northeastern United States.

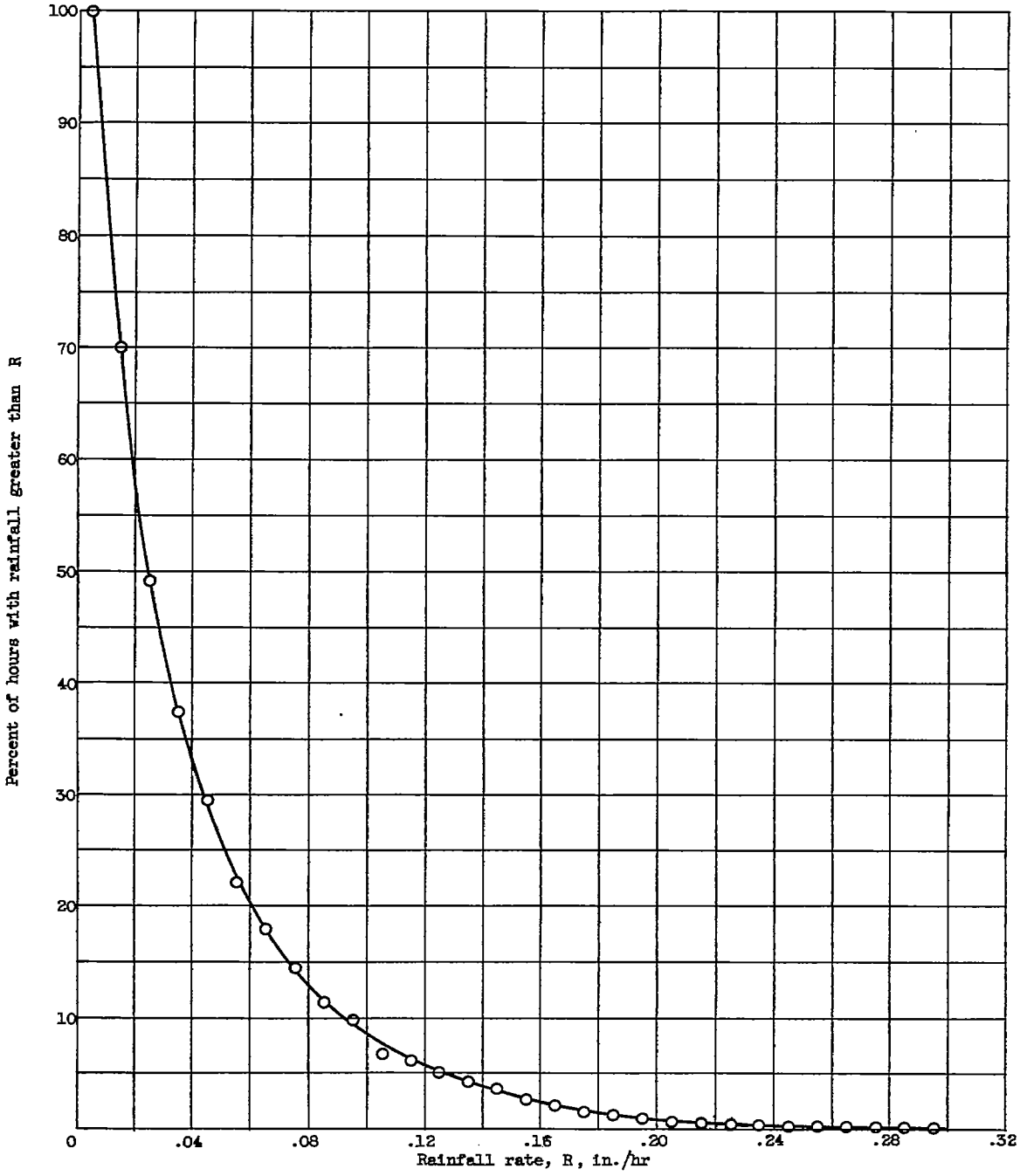

Figure 11. - Frequency distribution of hourly rainfall amounts in New England during December, January, and February. Distribution includes hourly rainfall amounts exceeding 0.005 inch recorded on days with maximum temperature of 45° F or lower and minimum temperature of 32° F or higher.

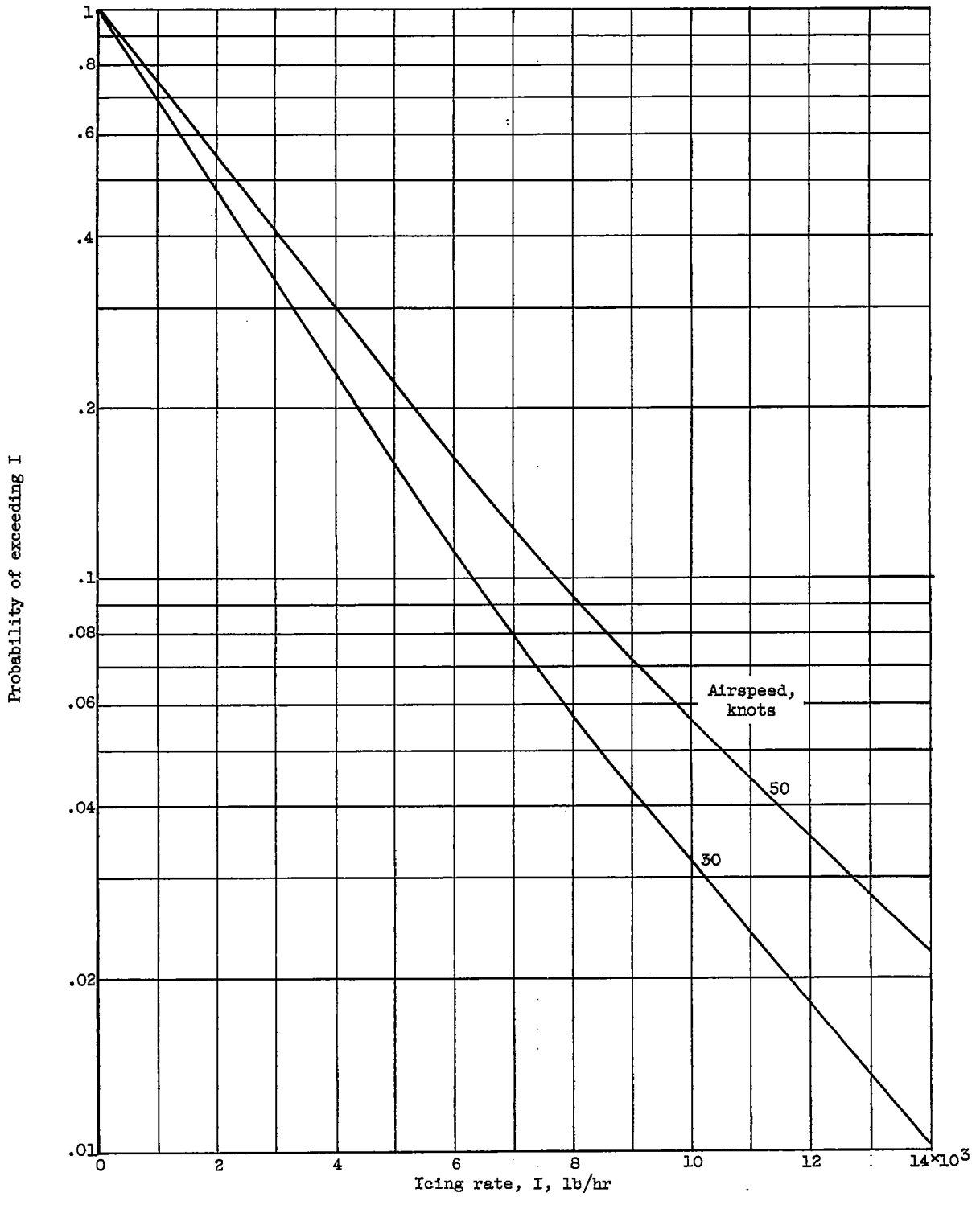

Figure 12. - Probability of exceeding various icing rates in northeastern United States during winter when flying in freezing rain.

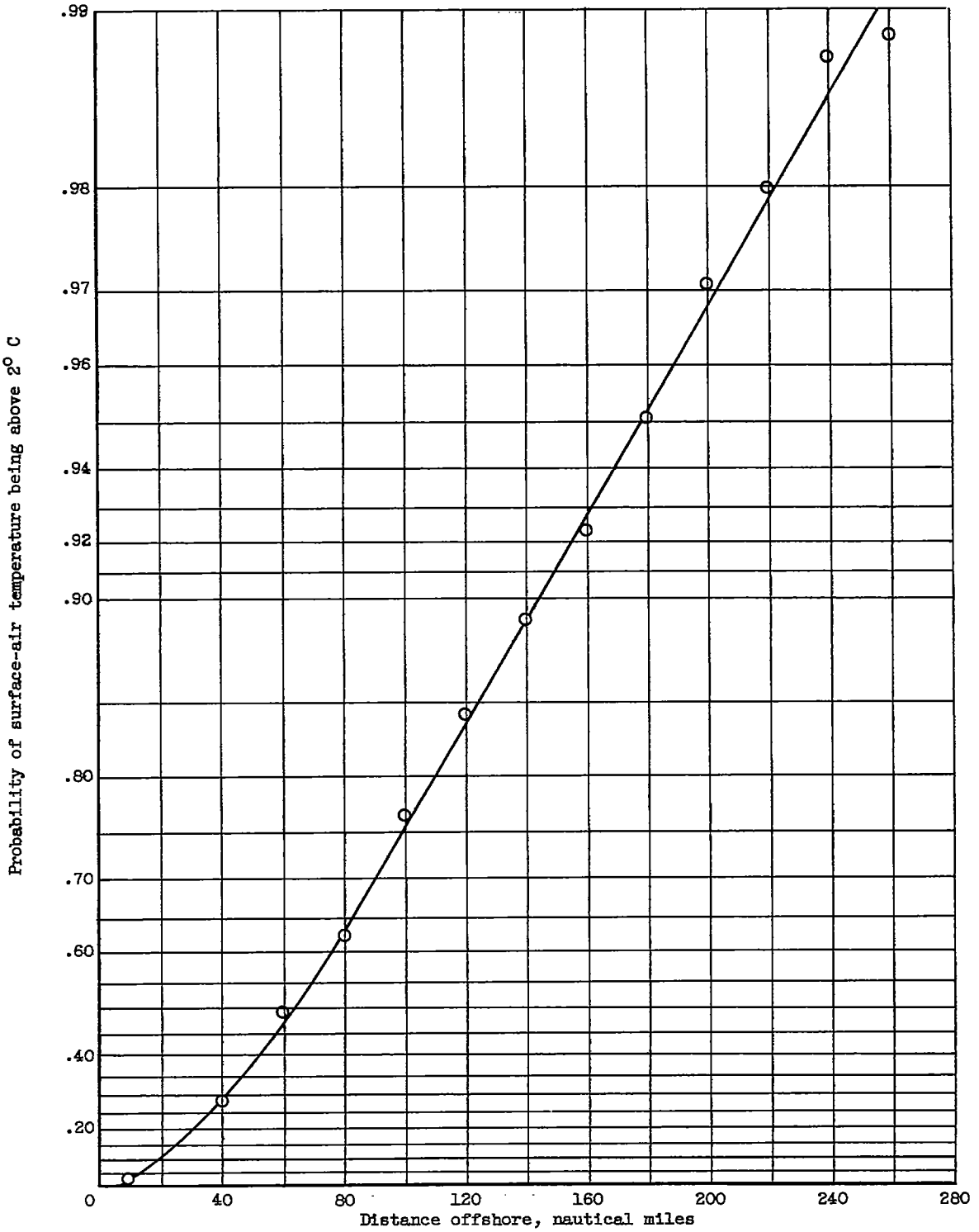

Figure 13. - Calculated heating effect of sea surface at 6° C on freezing-rain air-mass temperature.

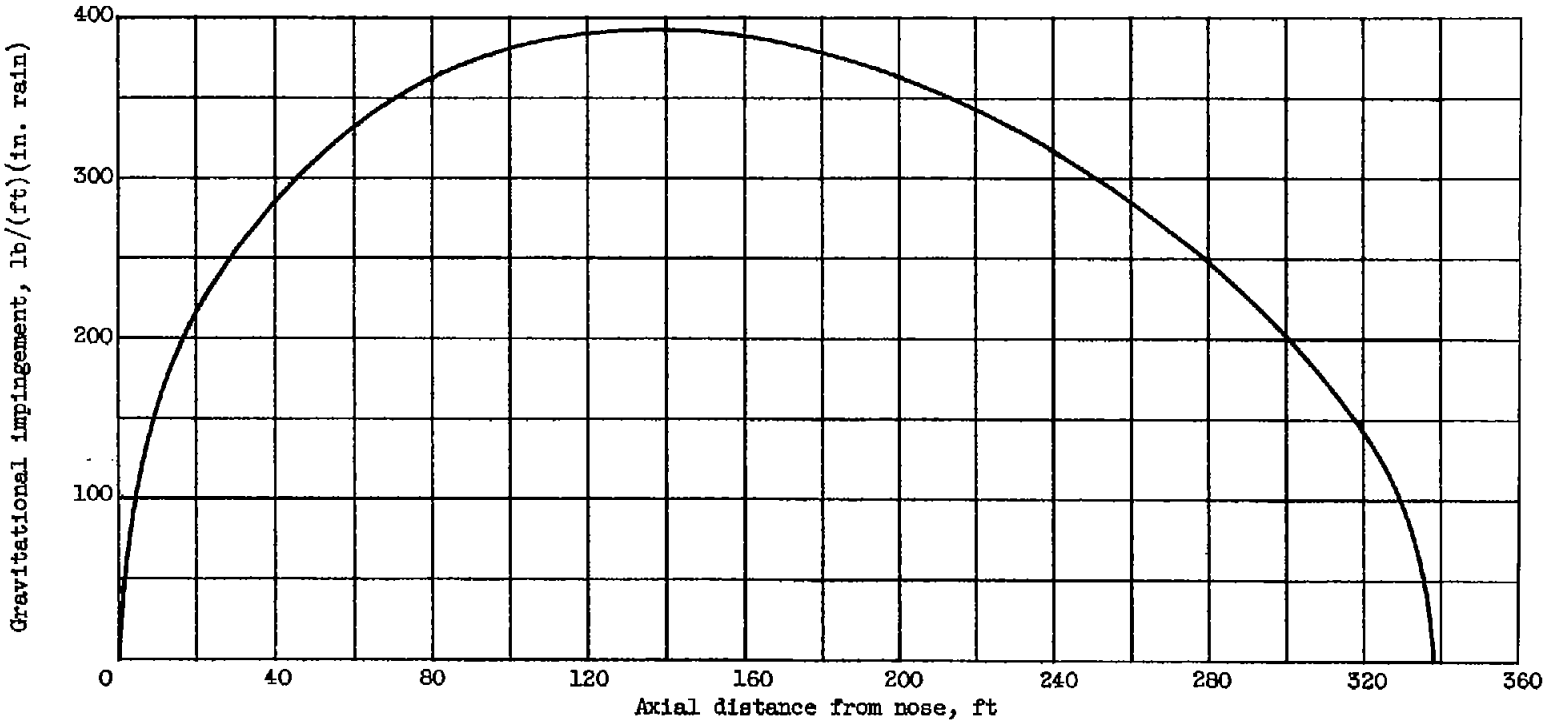

Figure 14. - Distribution of gravitational impingement.

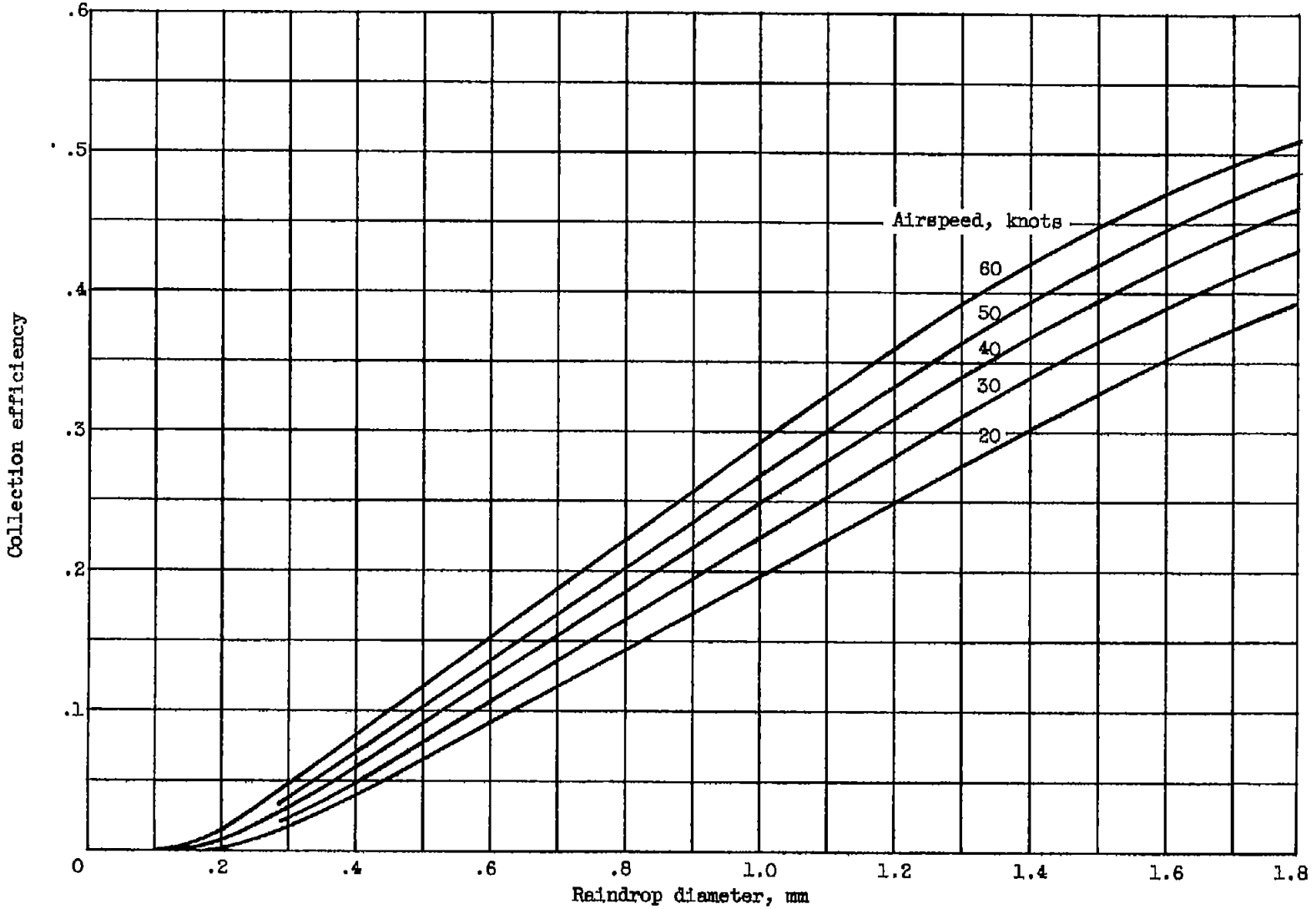

Figure 15. - Collection efficiency of airship in rain. Values calculated for ellipsoid of fineness ratio 3.25 with maximum diameter of 75.4 feet; pressure altitude, 3000 feet; temperature, -2° C; gravity neglected.

Figure 16. - Falling speed of raindrops at 3000 feet.

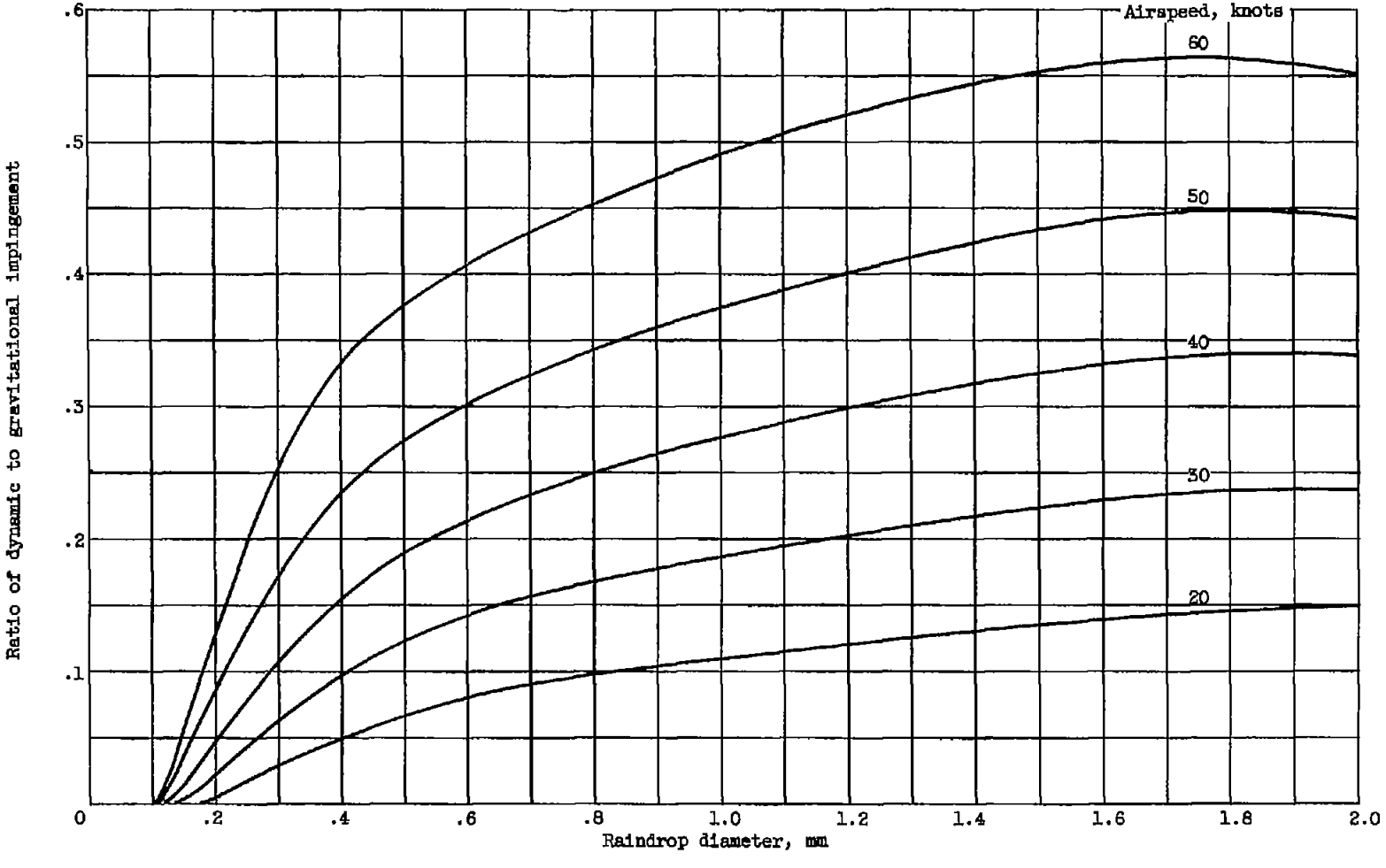

Figure 17. - Ratio of dynamic to gravitational impingement. Pressure altitude, 3000 feet; temperature, -2° C.

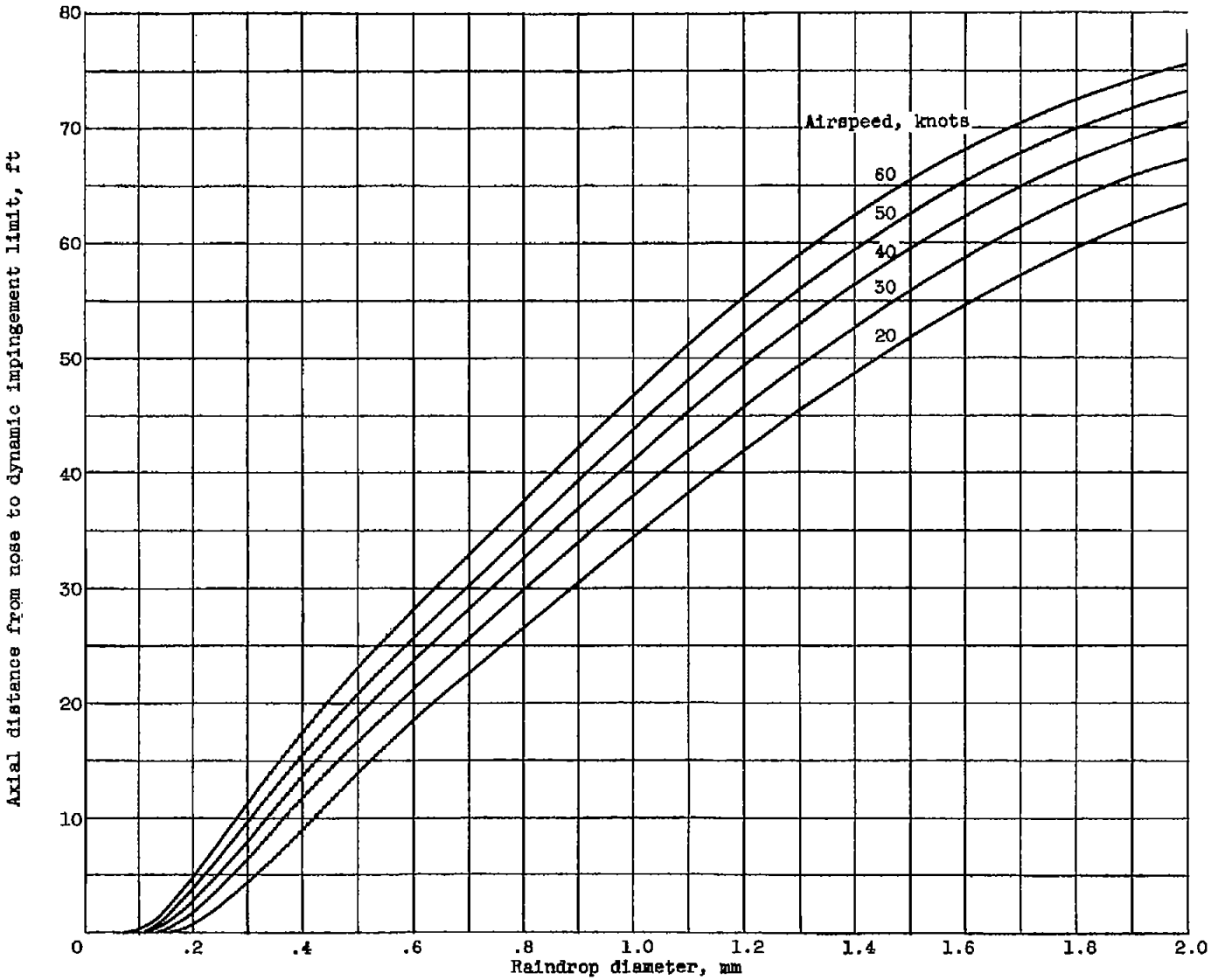

Figure 18. - Limit of dynamic impingement as function of raindrop diameter.

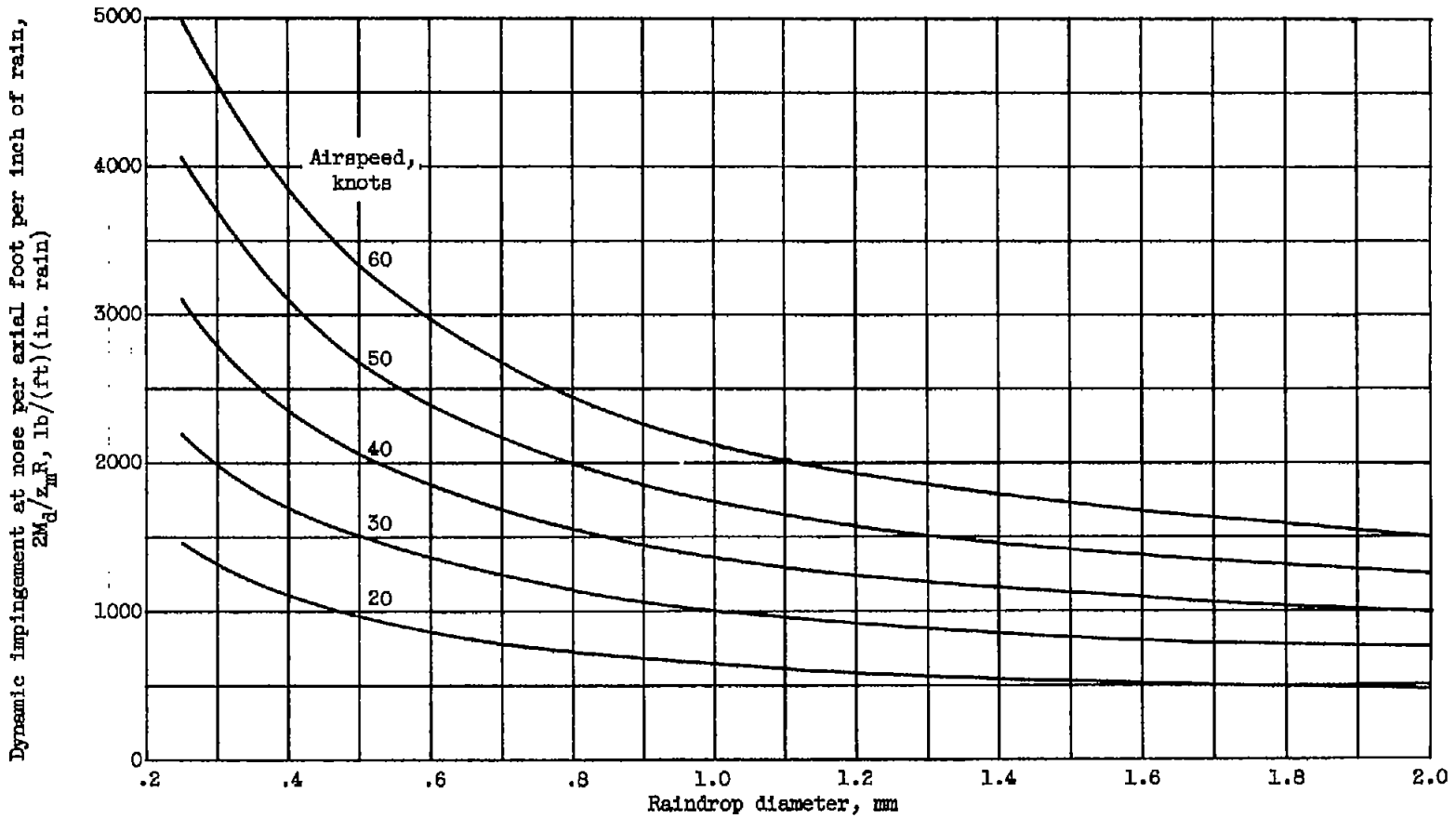

Figure 19. - Dynamic impingement at nose per axial foot per inch of rain.

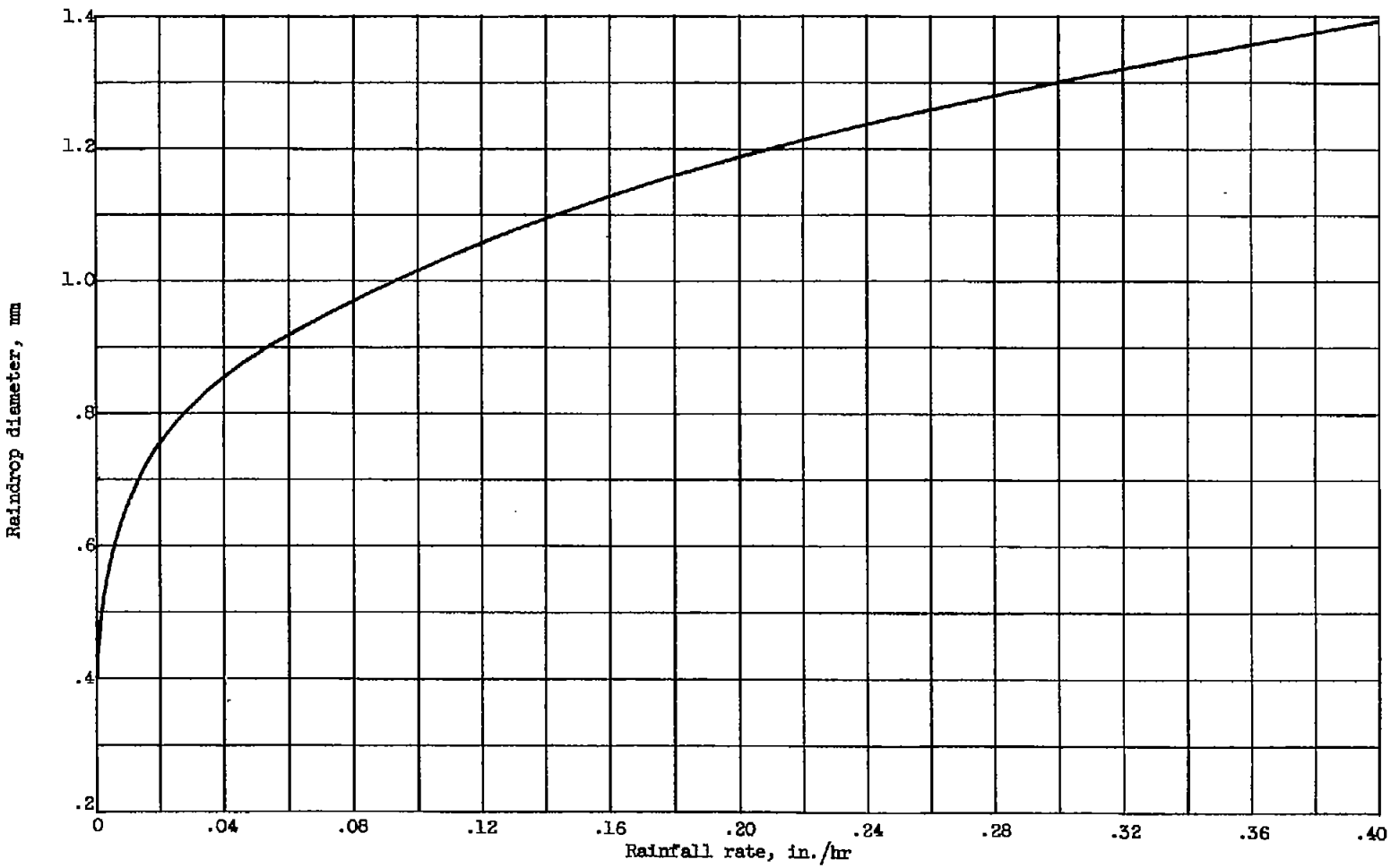

Figure 20. - Average raindrop diameter as function of rainfall rate (ref. 10).

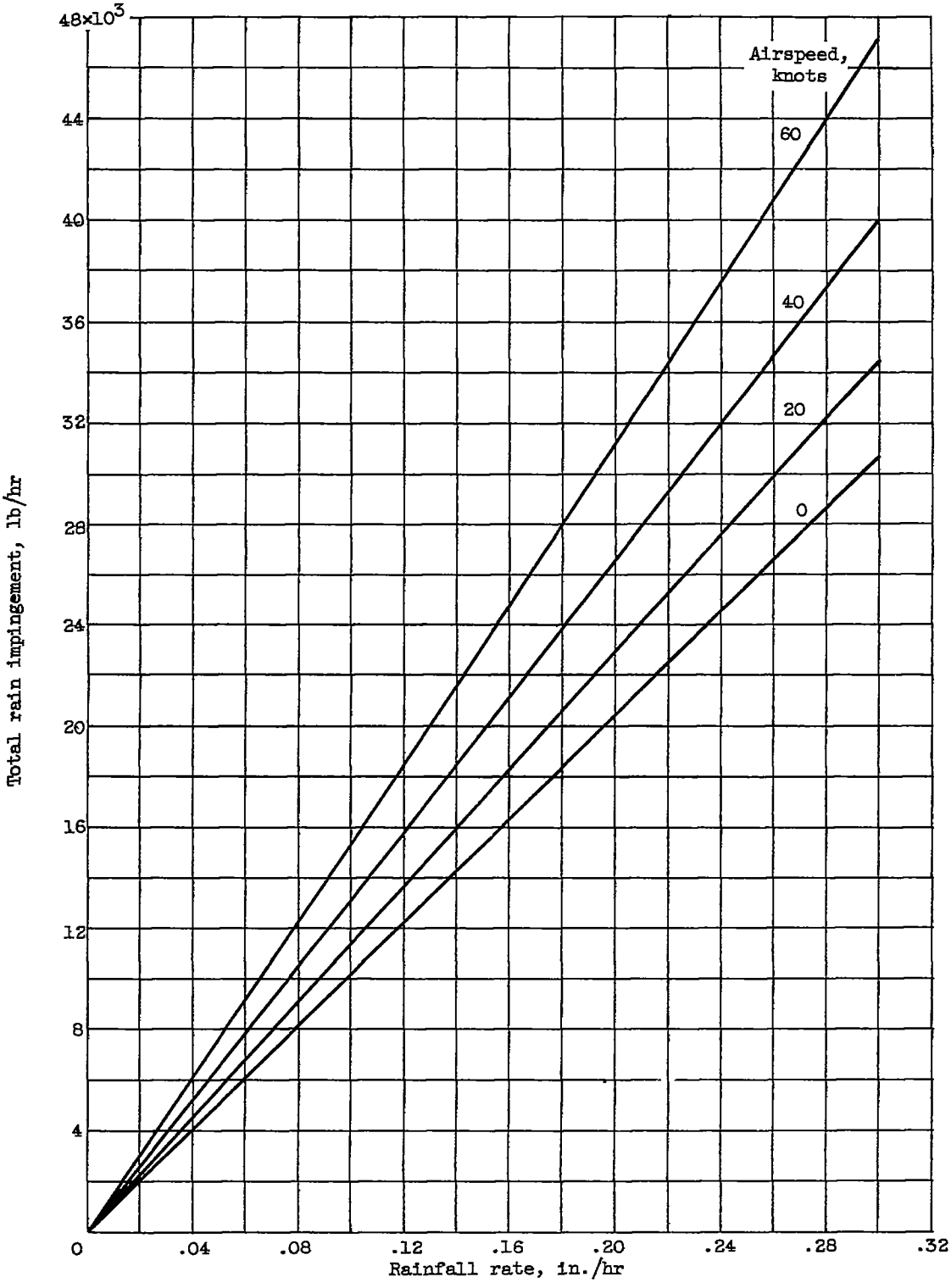

Figure 21. - Total rain impingement.

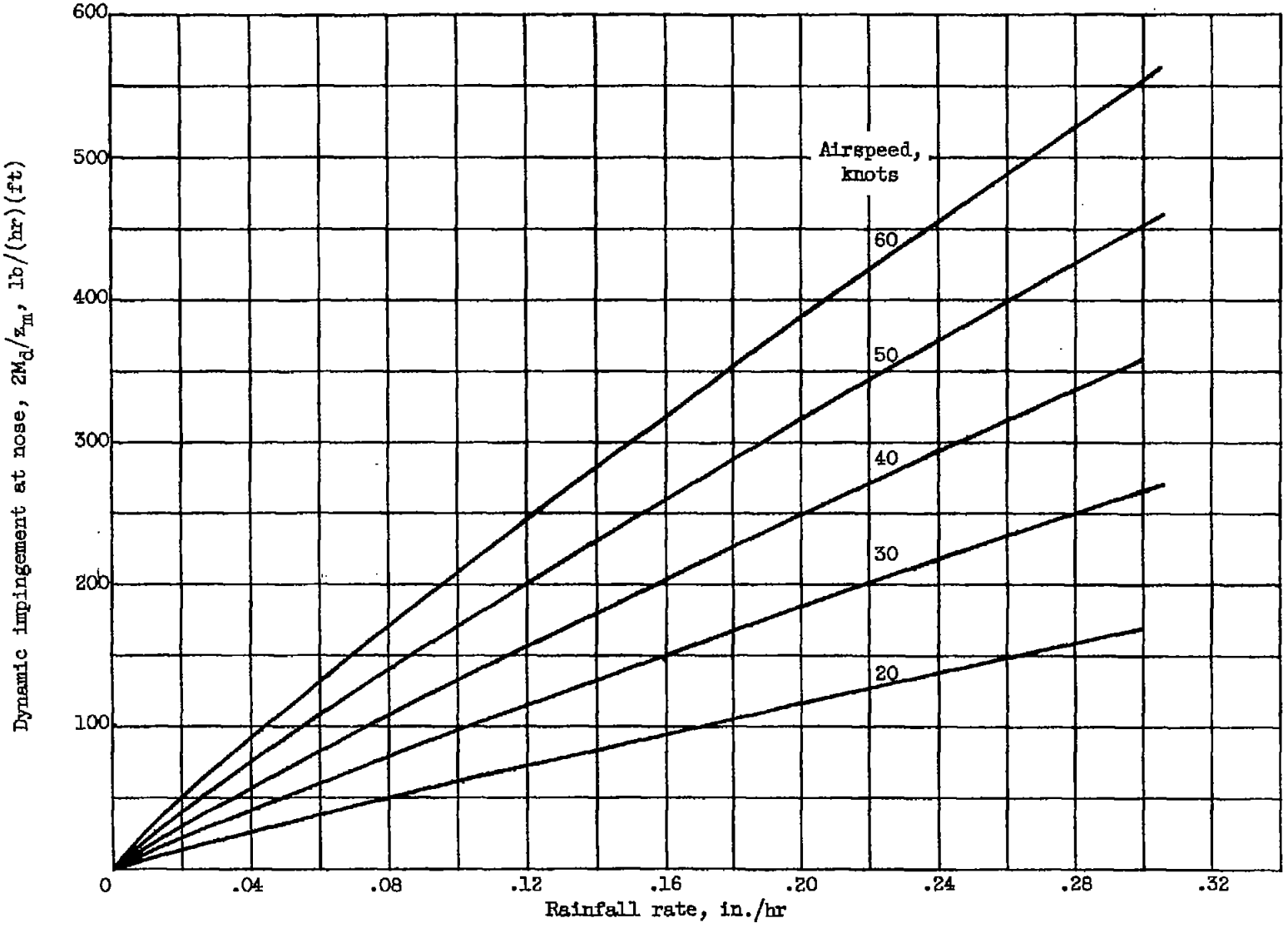

Figure 22. - Local dynamic impingement at nose.

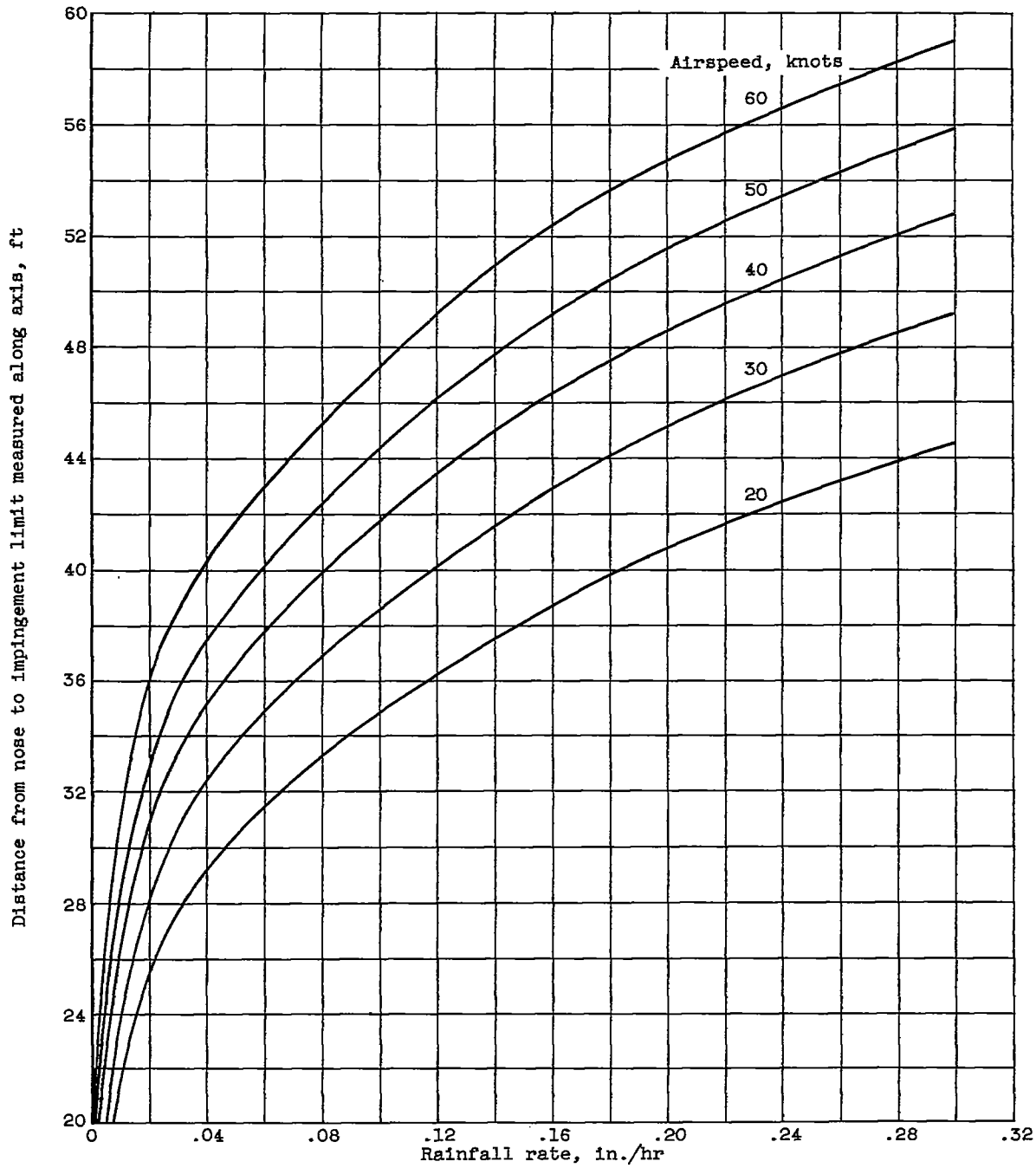

Figure 23. - Limit of dynamic impingement as function of rainfall rate.

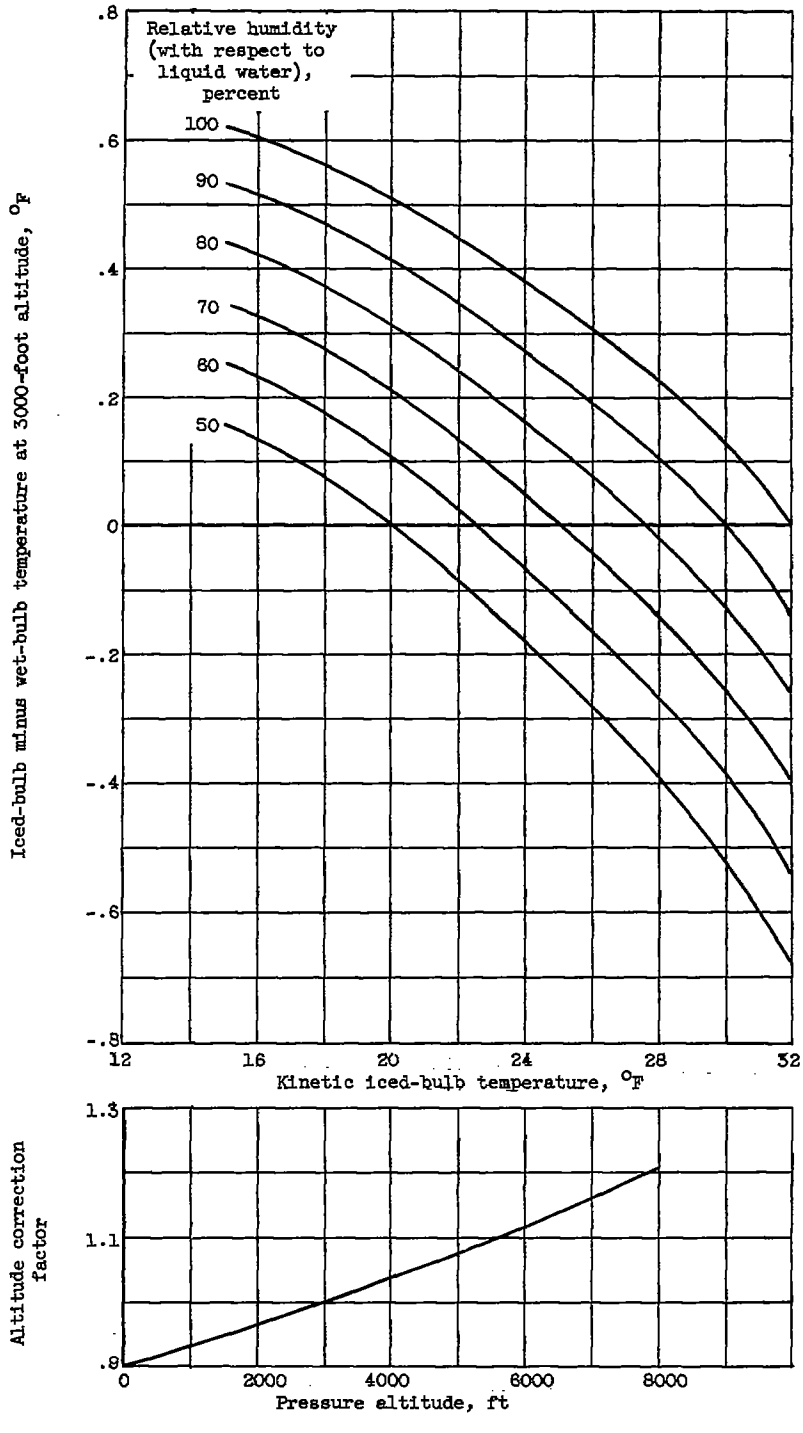

Figure 24. - Corrections to be subtracted from iced-bulb temperature to obtain wet-bulb temperature with respect to liquid water when wet-bulb thermometer is ice coated. Customary procedures for reducing aircraft psychrometric observations yield relative humidity with respect to liquid water when wet bulb is ice coated.

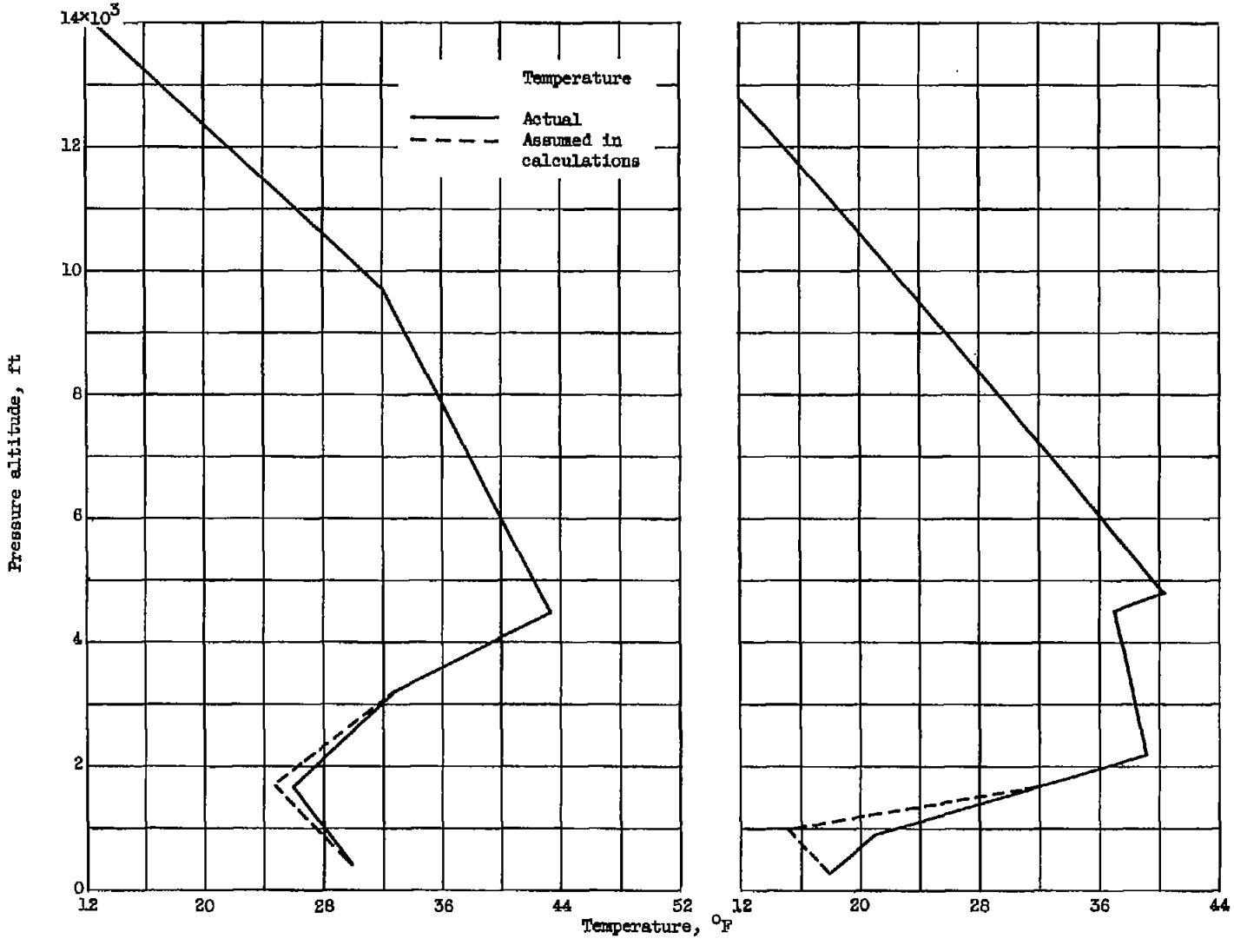

(a) Washington, D.C.; Jan. 9, 1956, 4:00 p.m., e.s.t.

(b) Albany, N.Y.; Jan. 9, 1956; 4:00 a.m., e.s.t.

Figure 25. - Examples of radiosonde observations during freezing rain.

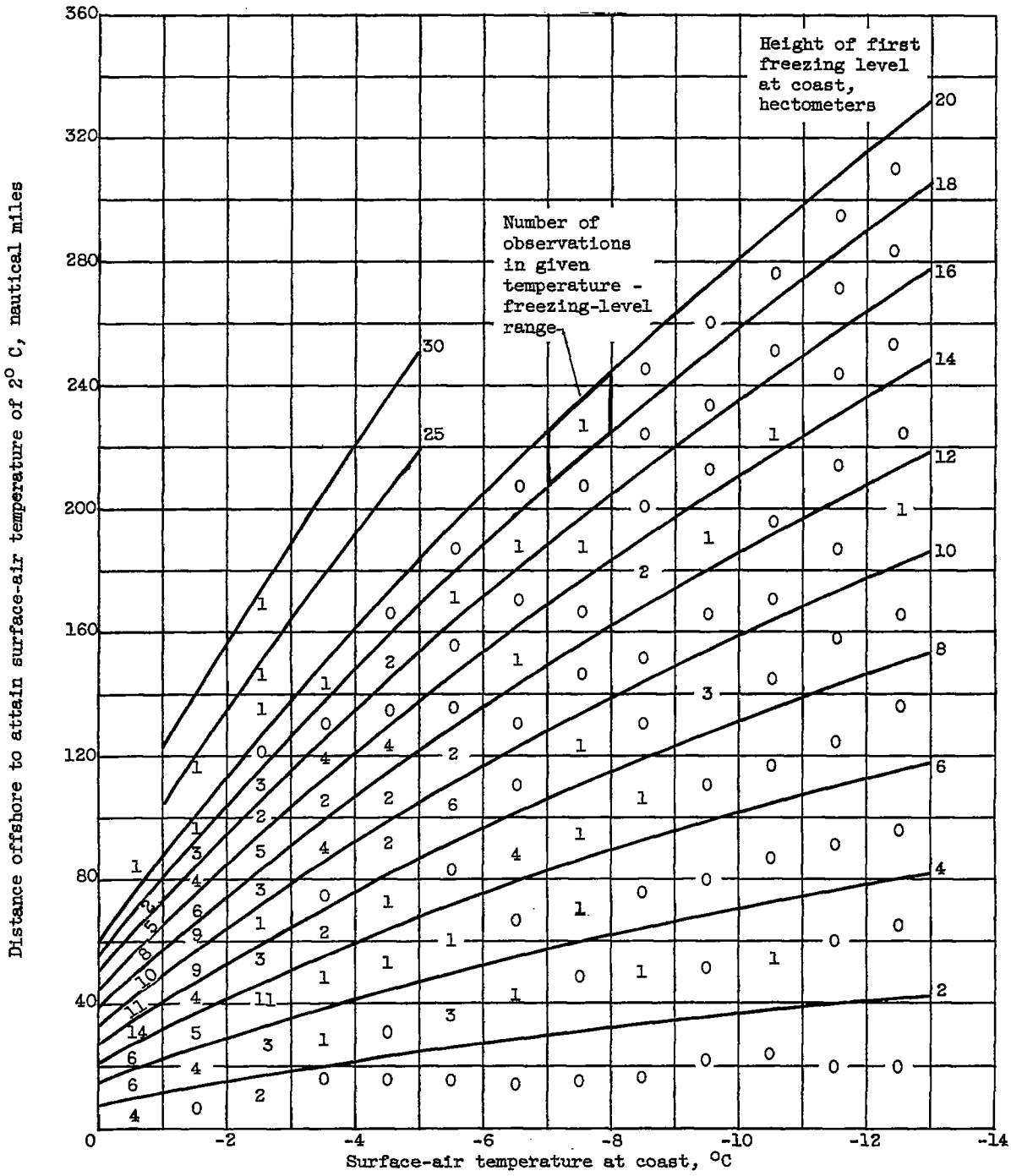

(a) Wind speed, 5 knots.

Figure 26. - Distance of flow over water at 6° C to attain surface-air temperature of 2° C as function of initial surface-air temperature and height of first freezing level.

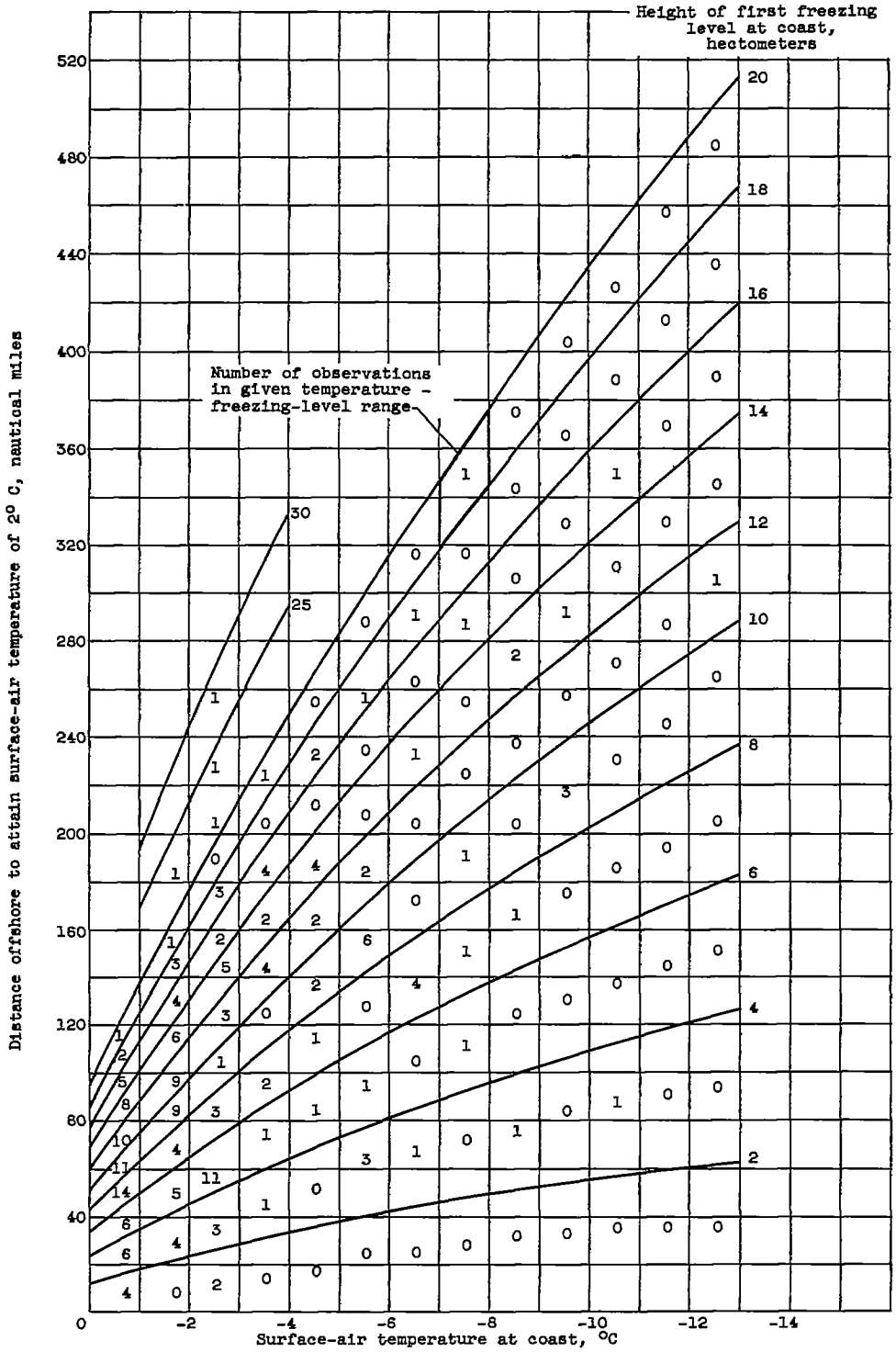

(b) Wind speed, 10 knots.

Figure 26. - Continued. Distance of flow over water at 6° C to attain surface-air temperature of 2° C as function of initial surface-air temperature and height of first freezing level.

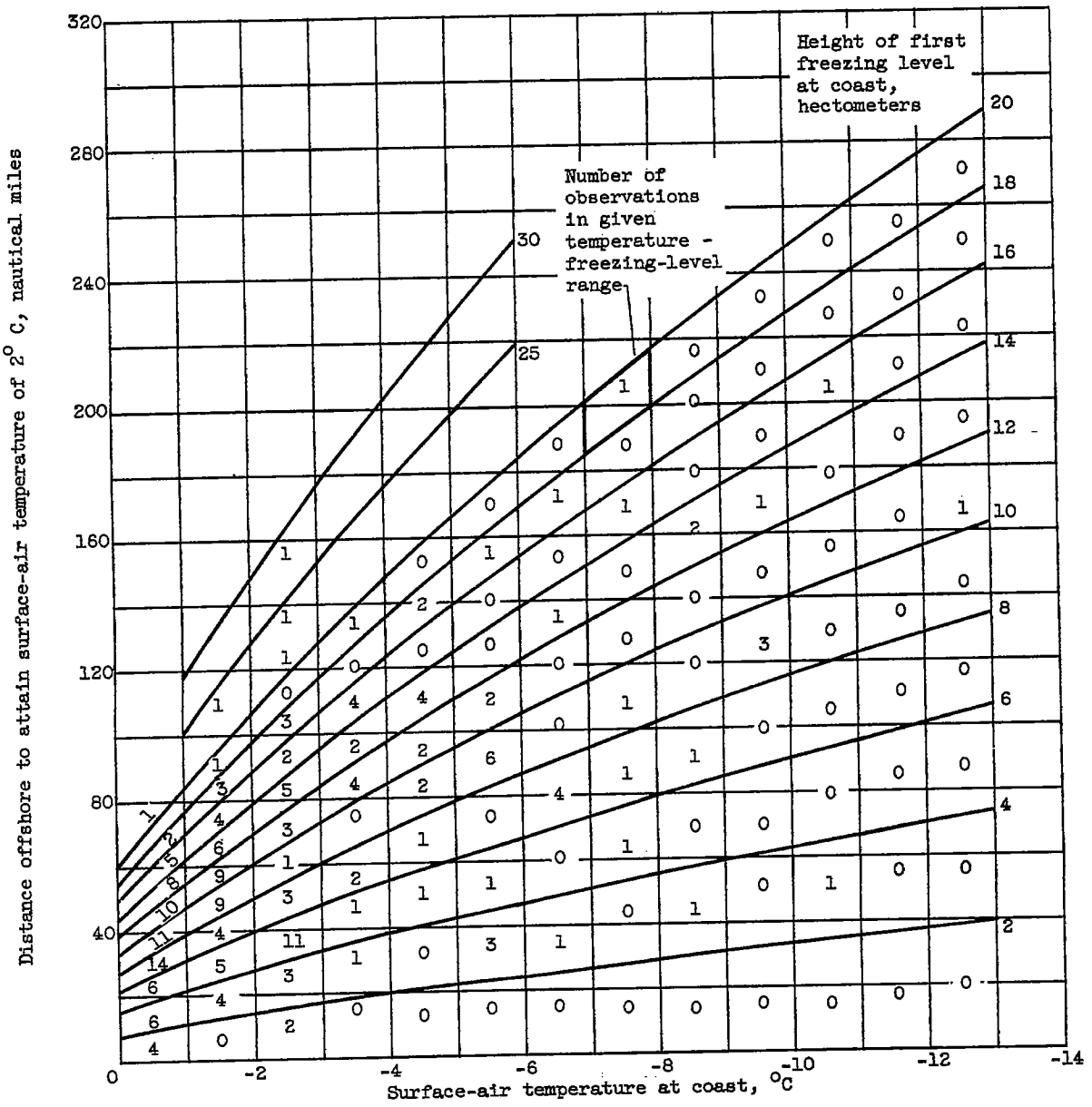

(c) Wind speed, 20 knots

Figure 26. - Concluded. Distance of flow over water at 6° C to attain surface-air temperature of 2° C as function of initial surface-air temperature and height of first freezing level.